Medizinische Fakultät
der
Universität Duisburg-Essen

Aus dem

Institut für Molekularbiologie

Role of sphingolipids in the immune response against tumor after local radiation

I n a u g u r a l d i s s e r t a t i o n
zur
Erlangung des Doktorgrades der Medizin
durch die Medizinische Fakultät
der Universität Duisburg-Essen

Vorgelegt von
Ashraf Swaidan
Aus Syrien
2021

DOI: 10.17185/duepublico/74860
URN: urn:nbn:de:hbz:464-20211018-150928-1

Dekan: Herr Univ.- Prof. Dr. med. J. Beur

1. Gutachter: Herr Univ.- Prof. Dr. med. E. Gulbins

2. Gutachter: Herr Univ.- Prof. Dr. rer. nat. D. Engel

Tag der mündlichen Prüfung: 13. September 2021

Table of Contents

1. Introduction

1.1 Overview of irradiation

1.1.1 Physics of radiation

Radiation therapy has been used for the treatment of various malignancies for decades with curative or palliative intent. The absorption of energy from radiation in biologic material may lead to excitation or ionization. The raising of an electron in an atom or molecule to a higher energy level without actual ejection of the electron is called excitation. If the radiation has sufficient energy to eject one or more orbital electrons from the atom or molecule, the process is called ionization. The critical characteristic of ionizing radiation is the localized release of large amounts of energy, which is more than enough to break a strong chemical bond. The biologic effects of radiation result principally from damage to deoxyribonucleic acid (DNA), which is the critical target. If any form of radiation is absorbed in biologic material, there is a possibility that it will interact directly with the essential targets in the cells. The atoms of the target itself may be ionized or excited, thus initiating the chain of events that leads to a biologic change. This is called direct action of radiation. Alternatively, the radiation may interact with other atoms or molecules in the cell (particularly water) to produce free radicals that can diffuse far enough to reach and damage the critical targets. This is called the indirect action of radiation (Figure.1). The period between the breakage of chemical bonds and the expression of the biologic effect extends from hours to decades, depending on the consequences of the biologic effects. If cell death is the result, the biological effect may be expressed in hours to days. If the radiation damage is oncogenic, its expression as overt cancer may be delayed for decades. If the damage is a mutation in a germ cell leading to genetic changes, it may not be expressed for many generations.

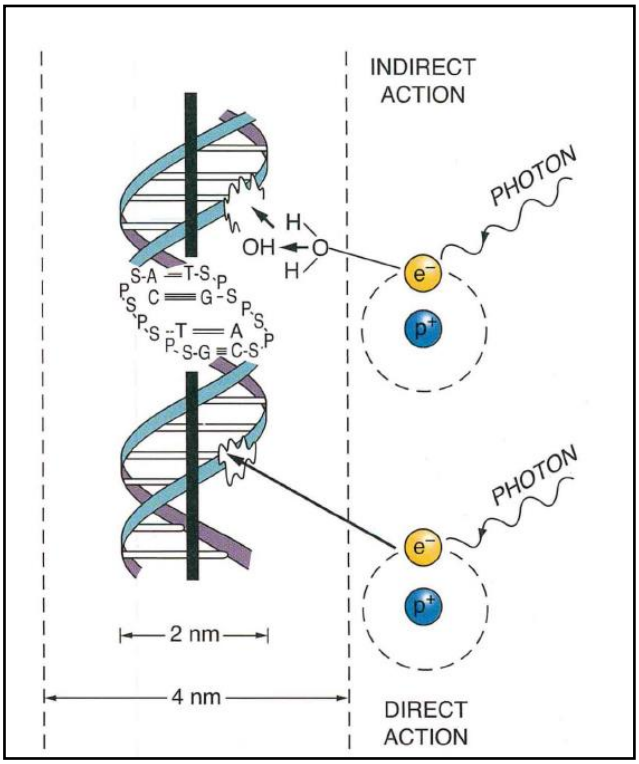

Figure 1. Direct and indirect actions of radiation

(Hall, radiobiology for radiologist's 7th 2012)

1.1.2 Advantages of radiation against tumorigenesis

Tumor radiotherapy is a technique that is used to control growth, metastasis, and proliferation of malignant tumor cells by using various types of ionizing radiation. Moreover, radiation can change the tumor immunogenicity, and microenvironment (Edimecheva et al., 1997, Shao et al., 2004), thereby globally altering the biological behaviour of cancer cells. During tumor treatment, radiation is considered to be a "double-edged sword" because it not only affects the tumor but may also genetically modify healthy tissues, causing damage to non- tumor cells. Apoptosis, necrosis, and senescence of cancer cells induced by DNA damage are the major effects of radiation on tumor tissue. Radiation directly causes DNA damage like single-strand breaks (SSBs), DSBs, DNA crosslinks, and DNA-protein crosslinks or induces damage indirectly to DNA by reactive oxygen species (ROS) or reactive nitrogen species (RNS)(Van Der Schans, 1978). Besides, exposure to radiation has a significant effect on the biological behaviour of the mitochondria in tumor cells. It can directly promote the release of cytochrome C by

releasing ROS or by indirectly triggering cytochrome C induced apoptosis through altering the permeability of the mitochondrial membrane (Kam and Banati, 2013). Radiation can directly cause corrosive damage to the cell membrane, which affects the permeability, integrity, and mobility, or indirectly alter the biological characteristics by affecting the composition of the cell membrane.

1.1.3 The abscopal effect after radiation

The abscopal effect refers to the regression of tumors that are outside the localized radiation treatment field, a phenomenon originally described by the British radiologist R.H. Mole in 1953. The abscopal effect (from the Latin “ab” away from and “scopus,” target) refers to the ability of localized radiation to trigger systemic antitumor effects, which are primarily immune-mediated (Demaria et al., 2004). Localized RT induces cell death and release of immunogenic factors through a process called immunogenic cell death (ICD), which triggers the release of several endogenous damage-associated molecular patterns (DAMPs). These DAMPs, which include calreticulin, high-mobility group box-1 protein (HMGB1), and adenosine triphosphate (ATP), contribute to the priming of the immune system by triggering dendritic cells (DCs), thus resulting in improved antigen presentation to T-cells (Grass et al., 2016) (Figure.2). Radiation also stimulates tumor cells to release chemokines CXCL16 and CXCL10, which boost the expression of adhesion molecules like E-selectin and ICAM-1 in endothelial cells, which facilitate the migration of lymphocytes to the irradiated tumor. Furthermore, radiated tumor cells upregulate major histocompatibility complex (MHC1), Fas, and NKG2D ligands, hence being killed by NK and T-cells (Chakraborty et al., 2003, Gameiro et al., 2014, Hallahan et al., 1996, Grass et al., 2016). Since radiation generates an immune response against the tumor represented by cross-presentation between the antigen-presenting cells (APCs), such as dendritic cells and cytotoxic T-cells (CTLs), Demaria and her co-workers hypothesized that the abscopal effect depends on T-cell recruitment. She verified this when she inoculated 67NR breast cancer in both flanks of C57BL/6 mice and treated the left one (radiated tumor) with a single dose of 6 Gy associated with an intraperitoneal injection of Flt3-L (to stimulate DCs proliferation and differentiation). The nonradiated tumor had significantly impaired growth. However, when the same method was implemented in nude mice lacking T-cells, there was no significant influence on the

nonradiated tumor (Demaria et al., 2004). Further, it was demonstrated that the abscopal effect depends on P53 upregulation after radiation.

Camphausen and coworkers implanted both Lewis lung cell carcinoma and T241 fibrosarcoma in the mid dorsum of wt and P53-ko mice and exposed the lower right leg to 5 fractions of 10 Gy. Tumor growth was delayed significantly in wt mice comparing to P53-ko mice. This effect was not tumor-specific but dose-dependent (Camphausen et al., 2003). Furthermore, some cases were published regarding abscopal effects in clinical cases. Okuma described an abscopal effect of radiation therapy in a 63-year-old patient who had undergone an extended hepatic right lobectomy. A follow-up exam after his surgery revealed a single metastasis in his right lung and a single metastasis in a mediastinal lymph node. Transcatheter arterial embolization was not permissible due to the hazards on his spinal artery. Therefore, external-beam irradiation, which was performed using an anteroposterior parallel-opposed technique, was focused on the mediastinal metastasis. Several CT scans were conducted after the radiation and revealed a reduction in the mediastinal metastasis; moreover, a shrinkage of the lung metastasis, which was out the radiation field, was observed (Okuma et al., 2011). Postow and colleagues reported a case about a patient who suffered from melanoma on her back and was treated with ipilimumab (a monoclonal antibody that inhibits an immunologic checkpoint on T-cells, CTLA-4). She underwent wide local excision of her primary lesion. Later on, she developed metastasis as paraspinal mass and right hilar lymphadenopathy. For this reason, ipilimumab was commenced as monotherapy with no improvement. Moreover, she witnessed an enlargement in the paraspinal mass and new splenic metastasis. In order to palliate her back pain, the paraspinal mass was irradiated along with ipilimumab, which led to significant shrinkage in the paraspinal mass. Surprisingly, her CT scan revealed regression in the lesions out of the radiation fields (splenic metastasis and right hilar adenopathy). This regression was constant for ten months after the treatment. Besides, changes in peripheral blood were observed after the combination therapy. They displayed higher titers of antibodies against NY-ESO1 (an antigen expressed in 40% of patients with advanced melanoma) proteins compared to monotherapy with ipilimumab, a rise in activated $CD4^+$ T-cells and a decrease in myeloid-derived suppressor cells (MDSC)(Postow et al., 2012).

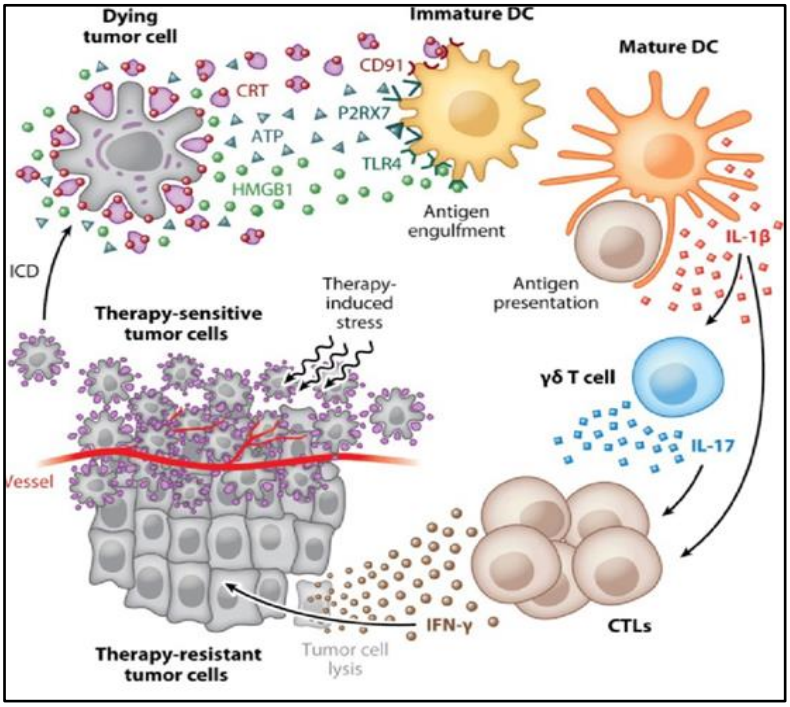

Figure 2. Triggering the immune response after radiation

Cellular injury may commence a waterfall of events inducing immunogenic cell death (ICD). Cells that experience ICD expose calreticulin (CRT) on the outer leaflet of their plasma membrane; moreover, the release high-mobility group box-1 protein (HMGB1) as necrosis permeabilized their cellular membrane. ATP, which is secreted during apoptosis, CRT and HMBG1 are recognized by the dendritic cells (DCs), which bind these molecules to initiate maturing and assembling in the tumor microenvironment. Next, antigen-presenting is modulated by DCs to T-cells, and an immune response is produced to eradicate the tumor and perhaps induce an abscopal effect. (Guido Kroemer. et al. 2013).

1.2 Sphingolipids

1.2.1 Overview

Sphingolipids are structural molecules of cell membranes with essential roles in maintaining barrier function and fluidity (Futerman and Hannun, 2004). Sphingolipids also regulate various biological processes, such as proliferation, migration, and apoptosis (Dyatlovitskaya and Kandyba, 2006, Furuya et al., 2011, Gulbins and Kolesnick, 2002). Ceramide, the central molecule of sphingolipid metabolism, generally mediates anti-proliferative responses such as autophagy, senescence, and induction of apoptosis. Ceramide is composed of a sphingosine long-chain base (LCB) containing 18 carbons, which is amide-linked to a fatty acyl chain containing variable numbers of carbons, ranging from 14 to 26. Ceramide is hydrolysed by ceramidase (CDase) to yield sphingosine, which is phosphorylated by SPHK1 or SPHK2 to generate S1P (Figure.3). Conversely to ceramide, S1P induces proliferation, angiogenesis, and metastasis. Decline in ceramide levels or increase in S1P levels are increasingly implicated in various stages of cancer pathogenesis. The generation and accumulation of ceramide can result from an increase in de novo synthesis, the hydrolysis of sphingomyelin by sphingomyelinase (SMase), and the salvage pathway (Figure. 4) (Ogretmen, 2006, Ogretmen and Hannun, 2004, Saddoughi et al., 2008). Activation of SMase is the predominant pathway for the generation of ceramide, according to their maximum activity at pH value they are named acid, neutral, and alkaline SMase (Brown and London, 1998, Kolesnick et al., 2000)

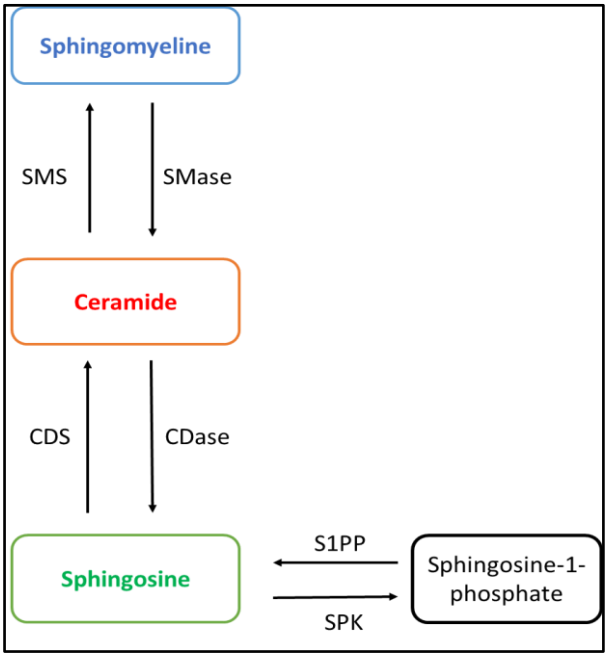

Figure 3. Sphingomyelin and its metabolism

Sphingomyelinase (SMase) catalyzes the hydrolysis of sphingomyelin to ceramide, ceramidase (CDase) catalyzes the hydrolysis of ceramide to sphingosine which is in turn transformed by sphingosine kinase (SPK) to sphingosine-1-phosphate (S1P). Controversially, sphingosine-1-phosphate phosphatase (S1PP) converts S1P to sphingosine which is converted to ceramide by ceramide synthase (CDS) and this last converted to sphingomyelin by sphingomyelin synthase (SMS).

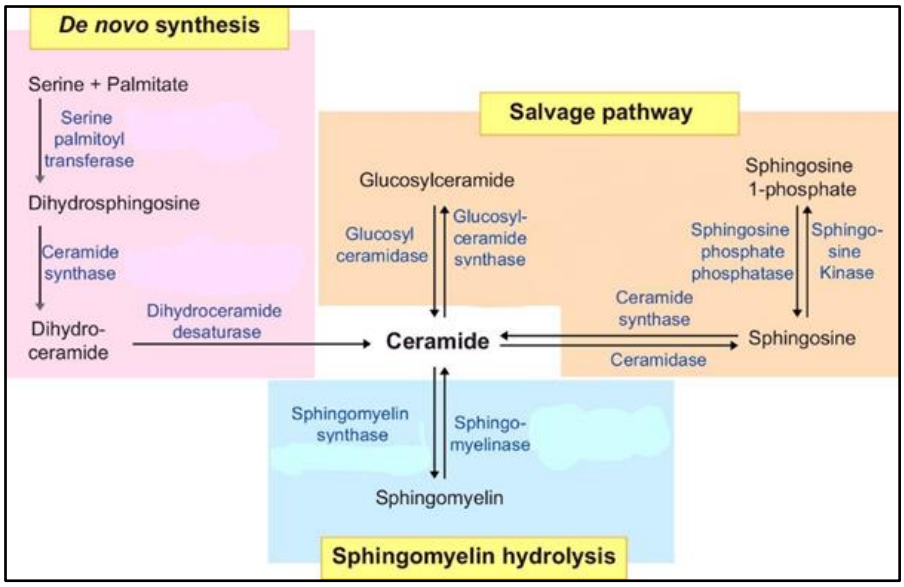

Figure 4. Ceramide biosynthesis pathways

(Modified from Yun-Chi Tang. et al. 2017)

1.2.2 Sphingolipids role in stress-induced apoptosis

CD95 receptors in cell membranes are death receptors, which are activated by different factors, such as interaction with CD95L on $CD8^+$ T-cells, TNF, INF-γ, and radiation (Grassme et al., 2001a). Acid sphingomyelinase (Asm), which localizes mainly in lysosomes, is transported upon the activation of CD95 by intracellular vesicles. These vesicles fuse with the cell membrane and expose the acid sphingomyelinase to the outer leaflet of the cell membrane. The activity of acid sphingomyelinase leads to release of ceramide and to the formation of ceramide-enriched platforms and the clustering of CD95 within these platforms. CD95 connects to the death domain (DD), which is essential for apoptosis initiation. The CD95/DD complex assembles the death-inducing signaling complex (DISC), which consists of CD95, the adaptor molecule FADD (Fas-associated with a death domain), procaspase-8, procaspase-10, and the caspase-8/10 regulator c-FLIP, and activate caspase 8 to initiate the apoptotic program (Grassme et al., 2001a, Grassme et al., 2001b). Oncogenes such as c-myc and p53 have essential roles in cell cycle control. Expression of c-myc induces cells both to proliferate and, in the absence of survival factors, to undergo apoptosis. Conversely, p53 induces cell cycle arrest and apoptosis. In an attempt to understand the mechanism through which ceramide mediates apoptosis in A20 cells, Bras et al studied variations in the expression of these proteins during ceramide treatment (Bras et al., 2000). He found that ceramide induced an increase in p53 and c-myc levels in A20 wt cells. The increase in p53 occurred 8 h after ceramide addition and was retained until 24 h; by 48 h after treatment, p53 decreased to normal levels. Concomitant with this p53 upregulation, he also observed a transient increase in c-myc after ceramide treatment. In contrast, p53 levels in A20Nur77 cells decreased after ceramide treatment, while c-myc levels remained unchanged. In contrast, anti-Fas treatment in both cell lines did not change p53 expression, indicating that p53 downregulation after treatment with ceramide is specific for the ceramide apoptosis pathway.

1.2.3 Sphingolipids and radiation

Radiation-induced Asm stimulation and subsequent ceramide generation are known to be involved in endothelial cell apoptosis. The molecular mechanisms regulating the endothelial response to high doses of radiation are suggested to be initiated via

translocation of endothelial Asm from the inner to the outer leaflet of the plasma membrane. Further, Asm catalyzes the hydrolysis of sphingomyelin to generate the lipid second messenger ceramide that leads to the transmembrane signaling of apoptosis (Gulbins and Kolesnick, 2002). Garcia Barros et al. (Garcia-Barros et al., 2003) demonstrated that MCA/129 fibrosarcoma and B16F1 melanoma cells implanted into $Asm^{-/-}$ mice show more than doubled growth rates comparing to tumors implanted in wt mice. Moreover, the radio-sensitivity of MCA/129 fibrosarcoma and B16F1 melanomas was dependent on host Asm. This was illustrated when irradiating tumors with a single dose of 15 Gy caused a growth delay in wt mice but did not affect tumors implanted into $Asm^{-/-}$ mice. At 15 Gy, fibrosarcoma in wt mice continued to grow for 2 to 3 days after irradiation, but after that displayed a reduction in size. In contrast, these tumors appeared completely resistant to 15 Gy when implanted in $Asm^{-/-}$ mice. To determine whether differences in tumor response to radiation correlated with the induction of endothelial apoptosis, the authors stained tumor tissue specimens with TUNEL and anti-CD34 after exposure to 15 Gy and found a markedly increased endothelial apoptosis in wt mice. In contrast, endothelium of tumors in $Asm^{-/-}$ mice were resistant to radiation-induced apoptotic death. Even at 20 Gy, enhanced endothelial apoptosis was not detected in tumors growing in $Asm^{-/-}$ mice, even though this dose overcame tumor radio-resistance in these mice, which indicates alternative mechanisms leading to delayed tumor growth in $Asm^{-/-}$ mice at the higher doses.

Furthermore, it was shown that overexpression of Asm in B16F10 murine melanoma cells, which were subcutaneously injected and irradiated with 15 Gy, resulted in tumors that were up to twelve-fold smaller than irradiated control tumors (Smith and Schuchman, 2008). Moreover, when irradiated melanomas were initially treated with a single, peritumoral injection of recombinant Asm, tumors were up to threefold smaller. Treatment of cancer cells with recombinant Asm induces ceramide and decreases cell viability after irradiation, and this effect is markedly enhanced in an acidic environment (pH 6.5)(Smith and Schuchman, 2008, Vaupel et al., 1989). The in vivo effect of Asm was likely due to enhanced cell death of the tumor cells themselves, as well as the surrounding microvascular endothelial cells. The Asm secreted from the overexpressing tumor cells impacted the angiogenic endothelial cells and led to fewer endothelial vessels per microscopic field two weeks post-irradiation (Smith and Schuchman, 2008).

1.2.4 Sphingolipids and metastasis

Sphingolipids also play a role in adhesion. Carpinteiro et al. demonstrated that intravenous injection of B16F10 melanoma cells in wt mice prompted pulmonary metastasis. In contrast, $Asm^{-/-}$ mice were preserved from hematogenous metastasis. This effect was due to an interaction between melanoma cells and platelets, leading to an activation of Asm and its releases from platelets to produce ceramide, leading to the formation of ceramide enriched platforms and the clustering and activation of α5β1 integrins in the cell membrane of melanoma cells which enables the melanoma cells to adhere and migrate to form metastases (Carpinteiro et al., 2015).

1.2.5 Sphingolipids and immune response

The immune response to tumors is complicated complex matter. Cells of the immune system can inhibit tumor growth and progression through the recognition and rejection of malignant cells. Still, immune responses can also promote tumor cell growth and angiogenesis through the secretion of inhibitory cytokines and direct inhibition of T-cells in the tumor microenvironment (TME). An essential role of the immune system is to identify and eliminate tumors. Transformed cells of tumors express antigens that are not present on healthy cells; these antigens are called tumor-associated antigens (TAAs). The immune system recognized these antigens as not-self and mounts an immune response against tumor cells. The most useful response of the immune system against tumors is to kill the abnormal cells using CTLs. TAAs are presented by MHC class I molecules of the antigen presenting cells (APCs) such as dendritic cells (DCs), macrophages and B cells. This allows CTLs to get activated and proliferate to attack the strange tumor cells. NK cells also kill tumor cells by cytotoxicity, especially if the tumor cells have fewer MHC class I molecules on their surface than healthy cells. Upon activation, CTLs express on their surface the death activator designated Fas, the engagement of Fas/FasL pathway then mediates apoptosis of cancer cells. Another tactic to destroy the tumor cells is the degranulation of cytotoxic granules, perforin and granzymes from the activated CTLs into the synaptic cleft between CTL and tumor cell. The microenvironment of tumors presents a substantial barrier against the immune response to the tumor. The microenvironment of tumors is established through the coordinated activity of regulatory myeloid-lymphocytic cells, as well as the elaboration of immune suppressive factors by tumors

themselves. Many tumor-infiltrating macrophages show an immune-suppressive nature. These macrophages, referred as myeloid-derived suppressor cells (MDSCs), mediate immune suppression through two enzymes involved in arginine metabolism: arginase 1 and nitric oxide synthase (NOS). In addition to myeloid cells, regulatory T-cells (Tregs) heavily infiltrate a diverse range of tumors. These cells, which express the transcription factor FoxP3 as well as CD4 and CD25, can suppress immune responses through the suppressive cytokines TGF-β and IL-35. The presence of Treg infiltration correlates with poor prognosis in several types of cancer. In addition to infiltration by regulatory immune cells, tumor cells often secrete immunosuppressive cytokines themselves, including IL-10, TGF-β, and VEGF. These cytokines not only inhibit cytotoxic immune responses but may also promote the formation or recruitment of additional regulatory cells (Martin et al., 2016). Efficient T-cell activation requires the cooperative engagement of at least two signals; the first signal is generated upon engagement of the TCR with the antigen-MHC complexes, and the second is the costimulatory signal which results from the interaction of CD28 with its ligands CD80/CD86 on the APC. It was shown by Boucher and his colleagues that CD28 triggers Asm activation, which results in ceramide accumulation in the plasma membrane. Ceramide is involved in the CD28 signal pathway of NF-kB and eventually in activating T-cells. Moreover, overexpression of recombinant Asm is shown to substitute for CD28 in the NFkB activation pathway. Accordingly, Asm is triggering by CD28 and offer an essential costimulatory signal for T-cell activation (Boucher et al., 1995). Besides the importance of co-stimulatory signals, a productive T-cell response also requires secretion of cytokines, such as IL-2, which is a major cytokine that promotes clonal expansion of T-cells. Sphingomyelin breakdown and ceramide generation appears to be involved in the release of IL-2 from T-cells since $Asm^{-/-}$ mice co-stimulated via the TCR and CD28 secreted less IL-2 than wt T-cells due to a dysfunction of the secretory vesicle system (Stoffel et al., 1998). Granule-mediated cytotoxicity is the central effector mechanism of cytotoxic T-cells (CTLs). The lytic effector molecules perforin, granzyme A and granzyme B are stored within granules of the CD8+ T-cells.

Upon TCR recognition of their antigenic peptide presented by MHC class I molecules on the surface of a target cell, the lytic granules are released into the synaptic cleft between the CD8+ T-cell and the target cell. Perforin liberated from these granules then forms holes in the cell membrane of the target cells to gain access to the target cell's cytoplasm,

where they induce apoptosis. However, the exocytosis of cytolytic effector molecules is diminished in $Asm^{-/-}$ mice. This was shown by delayed elimination of lymphocytic choriomeningitis virus from $Asm^{-/-}$ mice comparing to wt mice. The efficient expulsion of the granules requires an increase in membrane tension, which is physiologically achieved by Asm-mediated breakdown of sphingomyelin into ceramide (Herz et al., 2009). Ceramide also has a significant role in dendritic cell activation. A trial showed that infected DCs with lymphocytic choriomeningitis virus (LCMV) highly expressed MHC-I, MHC-II, B7-1, B7-2 and CD40, which means increased phenotypic maturation of DCs, when they were exposed to synthetic ceramide analog (C8). These activated DCs involved in priming the naive T-cells cell and their expansion (Pritzl et al., 2015). However, the surface expression of PD-L1 on DCs, which interacts with PD-1 on T-cells and deactivate them (Peng et al., 2020), was not affected by the addition of ceramide. Moreover, C8 ceramide did not induce cell death of DCs in vitro, in contrast to its known roles in the induction of apoptosis in tumor cells, which may consider administering ceramide as a therapeutic -immune agent is safe (Pritzl et al., 2015). Tregs are immunosuppressive cells and generally downregulate induction and proliferation of effector T-cells, maintain tolerance to self-antigens, and prevent autoimmune disease. However, high levels of Tregs in the tumor microenvironment are associated with poor prognosis in many cancers because Tregs suppress T effector cells and hinder the immune response against cancer. Asm plays an important role in the regulation of Treg development by regulating ceramide production. The data exhibited that $Asm^{-/-}$ mice had a significantly higher total number of Treg cells compared with wt in vivo. Additionally, the differentiation of $CD4^+$ T-cells into $Foxp3^+$ induced Treg (iTregs) in the presence of TGF-β and IL-2 led to a higher percentage of iTreg from $Asm^{-/-}$ compared with wt mice (Zhou et al., 2016). On the other hand, overexpression of Asm in T-cells results in a significant reduction in the number of Tregs within the spleen. Data from Hose et al. demonstrate that overexpression of Asm induces less differentiation of T helper cells into Tregs upon stimulation in the presence of IL-2 and TGF-β in vitro in comparison to wt. Moreover, T helper cells in Asm overexpressing mice differentiate more efficiently into IFN-γ producing Th1 cells than wt mice upon TCR engagement in the presence of IL-12 and IL-4. Additionally, infected t-ASM mice with Plasmodium yoelii exhibited significantly less parasitaemia than wt mice, indicating that enforced Asm activity in T-cells

contributes to elevated T-cell activation (Hose et al., 2019). Migration of effector T cells across blood vessels into tissues to fight tumor occurs via a multi-step pathway including lymphocyte rolling, signalling, firm adhesion and transmigration, which mainly depends on the adhesion molecule ICAM-1. The role of Asm in T-cells transmigration was mentioned by Lopes Pinheiro et al. and he found that endothelial ICAM-1 accumulation upon T cell interaction with the endothelium in the cerebral vessel is independent of the endothelial Asm. However, knocking out the Asm from the endothelial cell disrupts the T cells transmigration. Asm contributes to microvilli formation as ASM regulates ICAM-1 function in the endothelial cells, by controlling its interaction with filamin, and organizes the phosphorylation of ezrin (Pinheiro et al., 2016).

1.3 Aim of the study:

Based on the previous studies described above, sphingolipids play a role in regulating immune cells function through increasing the activation and proliferation of T-cells and DCs as well as decreasing Tregs. Moreover, sphingolipids and its main player ceramide play important roles in the apoptotic cascades of stressed cells. Therefore, we aim to define of acid sphingomyelinase and sphingolipids in tumor control after radiation.

2.Materials and methods

2.1 Materials

2.1.1 Cell line

Lewis lung carcinoma (LLC)	ATCC, Manassas, Virginia, United States

2.1.2 Media and additives:

DMEM	Thermo Fisher Scientific, Waltham, MA, USA
L-Glutamine	Thermo Fisher Scientific, Waltham, MA, USA
Non-essential amino acids	Thermo Fisher Scientific, Waltham, MA, USA
PenStrep	Thermo Fisher Scientific, Waltham, MA, USA
Sodium Pyruvate	Thermo Fisher Scientific, Waltham, MA, USA
HEPES/Saline (10×)	200 mM HEPES 1.32 M Nacl 10 M $CaCl_2$ 7 mM $MgCl_2$ 8 mM $MgSo_4$ 54 mM KCl pH was adjusted with HCl and NaOH to 7.4
Phosphate buffered saline (PBS)	137 mM NaCl 2.7 mM KCl 10 mM $Na_2HPO_4.2H_2O$ 2 mM KH_2PO_4 pH was adjusted with HCl and NaOH to 7.4

2.1.3 Kits & Anaesthesia:

Tumor Dissociation Kit, mouse	Miltenyi Biotec, Bergisch Gladbach, Germany
Matrigel Matrix	Corning, NY, USA
Mouse regulatory T-cell staining Kit	Thermo Fisher Scientific, Waltham, MA, USA
Mouse Cytokine Array Panel A	R&D Systems, Minneapolis, USA
Mouse/Rat CCL2/MCP-1 Quantikine	R&D Systems, ELISA kit, Minneapolis, USA
Mouse TIMP-1 Quantikine ELISA kit	R&D Systems, Minneapolis, USA
Ketamine 10%	medistar, Ascheberg, Germany
Xylazine 20mg/mL	Serumwerk Bernburg AG, Bernburg, Germany
Mouse Cytokine Array Kit, Panel A Summary	R&D Systems, Minneapolis, USA

2.1.4 Antibodies:

CD3 Per CP/Cy5.5 (anti mouse)	Biolegend, San Diego, CA, USA
CD19 Per CP/Cy5.5 (anti mouse)	Biolegend, San Diego, CA, USA
TER-119 Erythroid cells (anti mouse)	Biolegend, San Diego, CA, USA
Per CP/Cy5.5 (anti mouse)	Biolegend, San Diego, CA, USA
CD11b FITC (anti mouse)	Biolegend, San Diego, CA, USA
CD11C APC/Fire750 (anti mouse)	Biolegend, San Diego, CA, USA
Ly6G PE (anti mouse)	Biolegend, San Diego, CA, USA
Ly6C Alexa flour 700 (anti mouse)	Biolegend, San Diego, CA, USA
NK1.1 Alexa flour 647(anti mouse)	Biolegend, San Diego, CA, USA
F4/80 Brilliant violent 711 (anti mouse)	Biolegend, San Diego, CA, USA
CD8 PE/Cy7 (anti mouse)	Biolegend, San Diego, CA, USA
CD4 FITC (anti mouse)	Biolegend, San Diego, CA, USA
CD44 PE (anti mouse)	Biolegend, San Diego, CA, USA
CD19 PE (anti mouse)	Biolegend, San Diego, CA, USA
CD45 Brilliant violent 605 (anti mouse)	Biolegend, San Diego, CA, USA
CD25 APC (anti mouse)	Biolegend, San Diego, CA, USA
FOXP3 PE (anti mouse)	Biolegend, San Diego, CA, USA
Purified CD16/32 (anti mouse)	Biolegend, San Diego, CA, USA

2.1.5 Consumables:

Cell culture flasks	Sarstedt AG&CO, Nümbrecht, Germany
Cell strainer (70 µm)	Corning, NY, USA
Centrifuges tube (15mL, 50mL)	Greiner Bio-One GmbH, Frickenhausen, Germany
Insulin syringes	Becton Dickinson GmbH, Heidelberg, Germany
Pipettes different sizes	Nichiryo CO, Ltd, Saitama, Japan
Pipettus	Hirschmann Laborgeräte GmbH and CO.KG, Eberstadt, Germany

2.1.6 Equipment:

Digital calliper	Mitutoyo UK Ltd, Andover, UK
Evos cell imaging system	Thermo Fisher Scientific, MA, USA
Flow cytometer attune NXT	Thermo Fisher Scientific, MA, USA
Incubator	Binder GmbH, Tuttlingen, Germany
SCIL Vet abc	scil animal care company GmbH, Viernheim, Germany
Vortex (reax 2000)	Heidolph Instruments GmbH & CO.KG, Schwabach, Germany

Water bath	GFL Gesellschaft für Labortechnic mbH, Burgwedel, Germany
Freezers:	
-80 °C ultra-low MDF-U54V	Sanyo Electric CO, Osaka, Japan
-20 °C Premium NoFrost	Liebherr-International Deutschland GmbH
Fridge 4 °C, Premium BioFresh	Liebherr-International Deutschland GmbH

2.1.7 Software:

GraphPad Prism (8.1)	GraphPad Software, LA Jolla, CA, USA
Microsoft Office 2019	Microsoft Corporation, Redmond, WA, USA

2.2 Methods

2.2.1 Mice husbandry and breeding

$Asm^{-/-}$, tAsm and wt littermates were maintained on a C57BL/6J background and housed in the vivarium of the University Hospital Essen, Germany under pathogen-free conditions as defined by the Federation of European Laboratory Animal Science Association (FELASA). The $Asm^{-/-}$ mice were generated by insertion of a PGK-neomycin expression cassette into exon 2 of Smpd1 gene to disrupt the coding sequence of ASM, and they develop a phenotype that is identical to the Type A Niemann-Pick disease. Therefore, the $Asm^{-/-}$ mice and their wt littermates in this study aged only 6 to 8 weeks in order to avoid an accumulation of sphingomyelin. As for the tAsm mice, the mAsm gene is expressed under the control of the CAG ubiquitous promoter. The transgene activity depends upon the Cre recombinase-mediated excision of a STOP signal placed between the promoter and the cDNA. The transgenic construct was targeted to the Hprt locus. As the Hprt gene is localized to the X-chromosome, hemizygous male or homozygous females were chosen in our study (Horinouchi et al., 1995). Genotypes were assessed by PCR. Mice were maintained on a 12/12 light/dark cycle and had ad libitum access to food and water. All procedures were approved by the State Agency for Nature, Environment and Consumer Protection (LANUV) NRW in Düsseldorf, Germany.

2.2.2 Implantation of LLC cells

Upon receipt, cells were cultured in DMEM medium supplemented with 10% FCS, 10 mM HEPES, 2 mM L-glutamine, 1 mM sodium pyruvate, 100 µM non-essential amino acids, 100 U/mL penicillin and 100 µg/mL streptomycin in a confluency of 70% for up to four passages, screened to confirm the absence of mycoplasma contamination by PCR and aliquots were frozen in liquid nitrogen to create a batch of authenticated stock lines. Cell lines were defrosted and cultured to a limited passage (4-5) before implantation. Initially, the medium was discarded, and the cells were washed with PBS and treated with trypsin to dissociate them from the surface of the flask for 5 minutes, 37°C, 5%CO2. Later on, we added DMEM medium to undo the effect of trypsin, centrifuged at 300g for 5 minutes at 4 °C, discarded the supernatant and washed the cells with PBS for three times (resuspending the pellet with PBS and centrifuge 300 g / 5minutes / 4°C). The injection was under general anaesthesia with a Ketamine / Xylazine cocktail. A dose of 90 mg/kg Ketamine and 4.5 mg/kg was prepared by diluting Xylazine (20mg/mL) with 3,9 mL PBS, mixing 0.1 ml Ketamine (100 mg/mL) with 1 mL of the diluted Xylazine before administering the cocktail at a dose of 0.01 mL/g body weight via intraperitoneal injection. 5×10^4 cells /25 µL along with 25 µL of Matrigel (total volume 50 µL was mixed and filled in insulin syringes on ice) were inoculated subcutaneously in the right and left lower limbs.

2.2.3 Tumors radiation

Tumors were followed until they became palpable and irradiated when reaching a volume of (80 ±30) mm^3 by using an X-ray machine RS320 (Xstrahl Ltd) at 300 kV, 10 mA, and a dose rate of 0.9 Gy /minute. Tumor dimensions were measured via digital calliper and the volume was calculated depending on the following formula [(L×W×H)/2]. In $Asm^{-/-}$ mice the tumors displayed a slightly faster growth rate and reached the defined volume for radiation 11 days after implantation comparing to wt and tAsm mice which expressed tumors reaching a volume of (80 ±30) mm^3 after 13 days of implantation. In the analysis of the data, the tumor fold, which is the ratio of tumor volume after the respective day of radiation to the volume of the tumor on the day of radiation was determined and represents the tumor growth rate. Only tumors in the right lower limbs were radiated with a single dose of 15 Gy (primary tumors), whereas tumors in the left lower limb were not radiated

(secondary tumors). Placing a primary panel on the x-ray beam source enabled us to exclusively irradiate the right limb. Further, a shelter was installed to prevent radiation to other parts except for the right limb (Figure.5). During radiation, the mice were under anaesthesia by inhaling isoflurane.

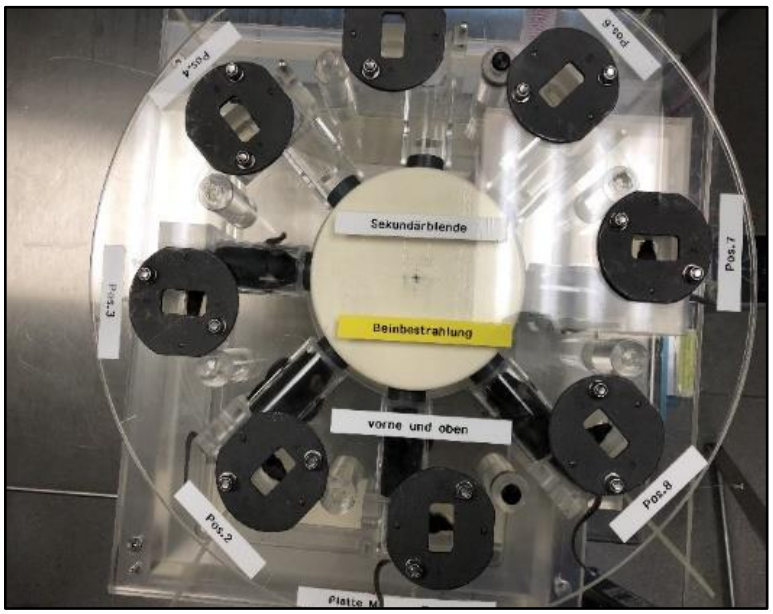

Figure 5. Radiation machinary
This figure illustrates how the mice were placed, and only the primary tumors were irradiated

2.2.4 Tumor, spleen, lymph nodes approach and analysis with flow cytometry

At two different endpoints, the mice were sacrificed by cervical spine dislocation. Tumors, spleen and inguinal lymph nodes were extracted and immune cells were analysed by flow cytometery. To obtain single-cell suspensions, tumors were processed using a gentle MACS dissociator and a murine tumor dissociation kit (Miltenyi Biotec), centrifuged at 400 g for 8 minutes at 4°C, the supernatant was discarded, the pelleted cells were resuspended in PBS+ (PBS with 2% FCS and 2mM EDTA), filtered by a 70 µm strainer, and centrifuged one more time. The pellet was resuspended in PBS+. Spleen and lymph nodes were smashed by a syringe plunger on a 70 µm strainer and resuspend with PBS+. Nonspecific FC-receptor binding was blocked first by incubation with purified CD16/32. Next, cells were incubated with conjugated antibodies (Table. 1) for 30 minutes

at 4°C in the dark, washed with PBS+, centrifuged at 300g for 5 minutes at 4°C. The supernatant was discarded, the cells were fixed in 4% PFA for 10 minutes at RT, washed with PBS, centrifuge at 300g for 5 minutes at 4°C, resuspend with1 mL PBS. For Tregs staining, the cell pellet was treated with 1 mL fixation/ permeabilization work solution at RT for 45 minutes in the dark, centrifuged with 300g for 5minutes at Rt, washed twice with 1 mL permeabilization buffer, centrifuged with 300g for 5 minutes at RT. The supernatant was discarded and the pellet was incubated with anti $FoxP_3$ for 30 minutes at RT in the dark, washed again with permeabilization buffer, centrifuged with 300g for 5minutes at RT, resuspend in 1 mL PBS. Samples were stored at 4°C to be analysed the following day by Attune NxT Flow Cytometer (Figure 6, 7, 8)

Table 1. A table displays the antibodies and their conjugated fluorescents with the proper dilutions

Antibody	**fluorescent**	**dilution**
anti CD3	PerCP/Cy5.5	1:200
anti CD19	PerCP/Cy5.5	1:200
anti CD11b	PerCP/Cy5.5	1:200
anti TER-119	PerCP/Cy5.5	1:200
anti CD45	briliant violet 605	1:200
anti CD11b	FITC	1:200
anti Ly6G	PE	1:400
anti Ly6C	Alexa flour 700	1:200
anti NK1.1	Alexa flour 647	1:800
anti CD11C	APC/Fire 750	1:200
anti F4/80	brilliant violet 711	1:200
anti IL-10	BV510	1:200
anti CD8	PE/Cy7	1:200
anti CD4	FITC	1:200
anti CD44	PE	1:400
anti CD19	PE	1:400
anti CD22	Alexa flour 647	1:800
anti CD25	APC	1:800
anti FoxP3	PE	1:100

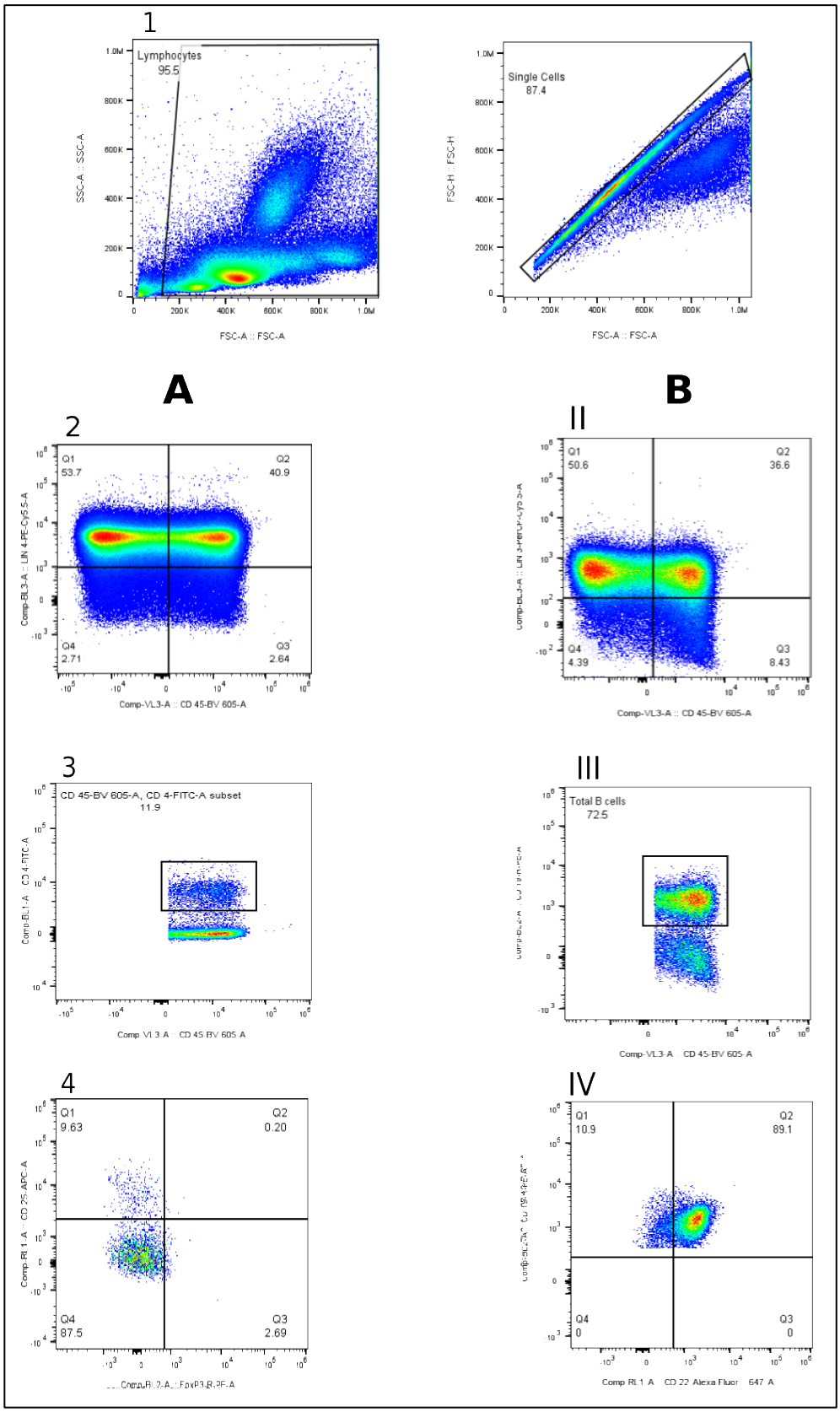

Figure 6. Gating strategy for the identification of mouse Tregs and B cell subsets

Lymphocytes were gated and the doublets were excluded (1). A) Gating strategy used to define Tregs in tumor, spleen and inguinal lymph nodes of C57Bl/6 tumor-bearing mice. Live CD45 cells were gated after excluding CD19 cells, CD11b cells and TER-119 (2 Q2). Total CD4 Th cells were gated (3) and from this gate, Tregs were gated according to the expression of CD25 and intracellular FoxP3 (4). B) Gating strategy used to define B cells in tumor, spleen and inguinal lymph nodes of C57Bl/6 tumor-bearing mice. Live CD45 cells were gated after excluding CD3 cells, CD11b cells and TER-119 (II. Q2). Total CD19 B cells were gated (III) and the activated B cells highly expressed CD 22 (IV).

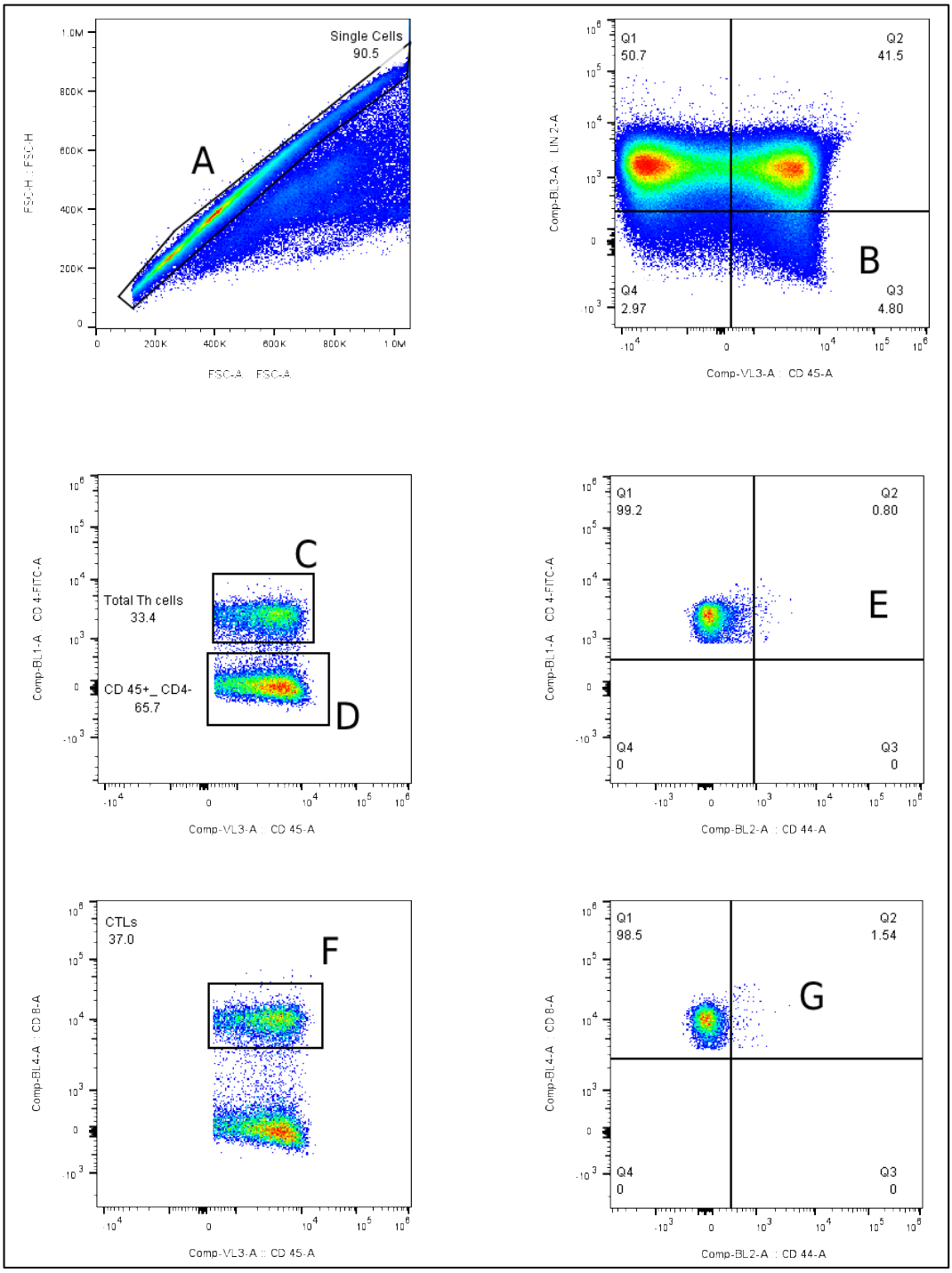

Figure 7. Gating strategy for the identification of mouse T cell subsets

Gating strategy used to define T cell subpopulations in tumor, spleen and inguinal lymph nodes of C57Bl/6 tumor-bearing mice. After exclusion of doublets (A), live CD45 cells were gated after excluding CD19 cells, CD11b cells and TER-119 red blood cells (B). From gate B, Total CD4 Th cells were gated (C) and the activated Th cells highly

expressed CD 44 (E). From gate D, total CTLs were gated (F) and the activated ones were highly expressed CD44 (G).

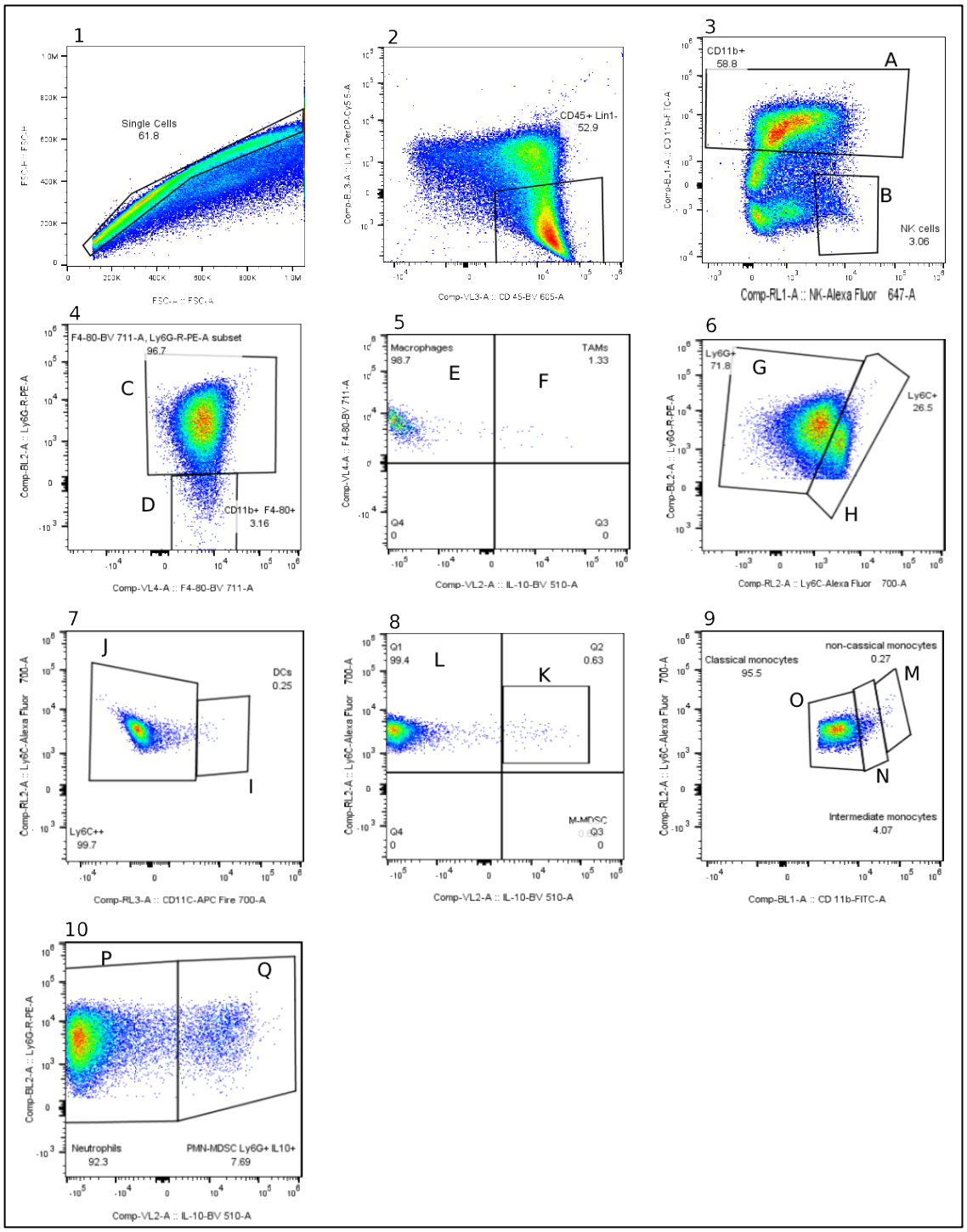

Figure 8. Gating strategy for the identification of mouse MDSCs

After excluding the doublets (1), CD45 cells were gated with excluding CD3 cells, CD19

cells and TER-119 red blood cells (2). From gate (2), CD11b myeloid cells (A) and CD NK1.1 NK cells (B) were gated. Gate (D) was descended from (A) and represented F4/80 cells and by Intracellular staining with IL-10, infiltrated macrophages and TAMs were gated E and F, respectively. Gate (G) was descended from the gate (C) and displayed Ly6G cells, which were intracellularly stained with IL-10 to differentiate between neutrophils (P) and PMN-MDSCs. Gate (H) was descended from the gate (C) and displayed Ly6C cells, which conclude CD11C dendritic cells (I) and highly expressed Ly6C cells (J). The intracellular staining differentiated the cells from the gate (J) to M-MDSCs (K) and infiltrated monocytes (L), which divides into three groups, non-classical monocytes (M), intermediate monocytes (N) and classical monocytes (O).

2.2.5 circulated WBCs assay in blood

10µL EDTA blood sampled were collected from the vein of tails at the end of the experiment and analysed through scil Vet abc to determine blood counts including leukocyte differentiation.

2.2.6 Cytokines assay in cytokine panel array A

Cytokines (BLC, C5/C5a, G-CSF, GM-CSF, I-309, Eotaxin, sICAM-1, IFN-γ, IL-1α, IL-1β, IL-1ra, IL-2, IL-3, IL-4, IL-5, IL-6, IL-7, IL-10, IL-13, IL-12 p70, IL-16, IL-17, IL-23, IL-27, CXCL10/CRG-2, CXCL11, CXCL1, CCL2/MCP1, CCL12, CXCL9, CCL3, CCL4, CXCL2, CCL5, CXCL12, CCL17, TIMP1, TNF-α, TREM-1) were analysed in serum samples. Blood samples were allowed to clot for 2 hours at room temperature before centrifuging for 20 minutes at 2000g. Serum was removed, and samples were stored at (-80 °C) to be assayed later. The following steps were proceeded according to the manufacturer's instructions.

2.2.7 Cytokines assay in serum

Blood samples were collected at the end of the experiment and left to clot for 2 hours at room temperature before centrifuging for 20 minutes at 2000g. Serum was taken and stored at ≤ -80 °C. Later, samples were thawed and diluted to proper concentration (1:6 for MCP1 and 1:15 for TIMP-1). 50 µL of assay diluent RD1-21 was added to each well of 96 well polystyrene microplate coated with a monoclonal antibody specific for mouse TIMP-1 or MCP-1. Afterwards, 50 µL of standard, control, or sample was added to each well and incubated for 2 hours at RT. Next step, aspiration and repeated wash was

performed for a total of five washes for each well with wash buffer. 100 µL of mouse TIMP-1 or MCP-1 polyclonal antibody conjugated to horseradish peroxidase was added to each well and incubated for 2 hours at RT. The conjugated antibodies were aspirated and each well was washed for a total of five washes with wash buffer. 100 µL of stop solution was added to each well, and analysis was performed by using a microplate reader set to 450 nm with a correction set to 540 nm.

3. Results

3.1 Ionizing radiation induces dose dependent cell death

To determine the dose-dependency of cell death of Lewis lung cell carcinoma (LLC) upon radiation, cells were seeded in gelatine-coated 6 well plates and irradiated with different doses (0,1, 2, 4, 8 Gy). After 7 days, colonies were counted using an Evos cell imaging system (Figure. 9). The results show a significant dose dependent decrease in colony-forming units when compared to non-irradiated cells, i.e., 0 Gy.

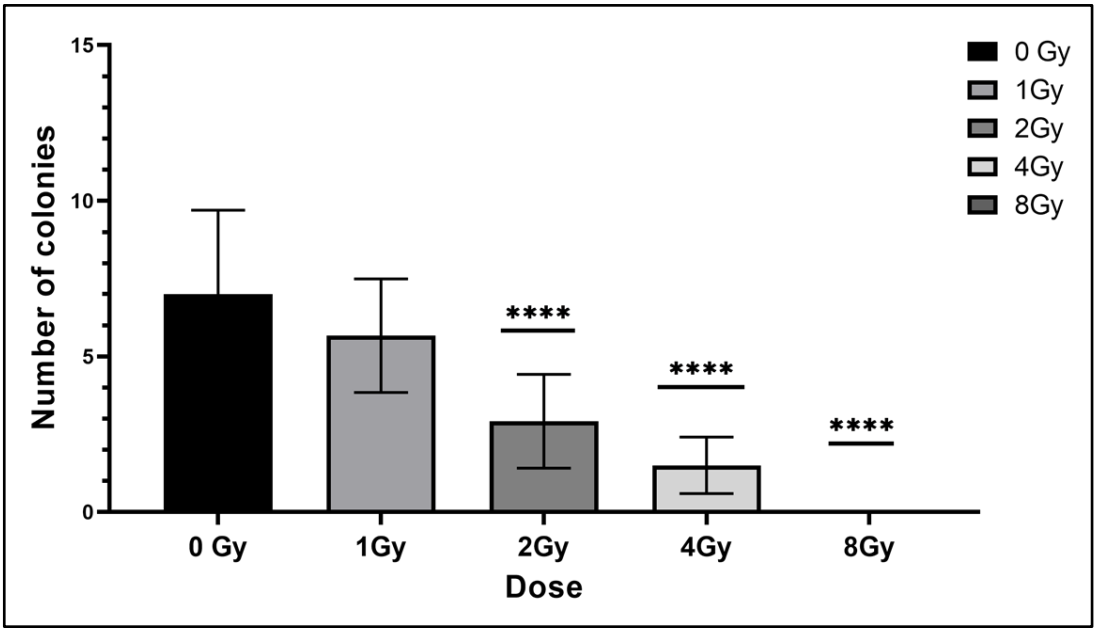

Figure 9. Dose dependant cell death upon radiation

200 cells were seeded in gelatine-coated 6 well plates and irradiated with different doses (1,2,4,8 Gy). After 7 days, colonies were counted under a Evos cell imaging cell system, considering that a colony consists of 50 cells or more. The data given are the mean values ± SD. Statistical significance between non-irradiated and irradiated cells was determined by analysis of variance (one way-ANOVA) followed by Bonferroni's selected comparisons test. P-values ($p \leq 0.0001$) are indicated by asterisks ****, n=6.

3.2 The effect of radiation on tumor growth in vivo

To investigate whether Asm in the host/tumor microenvironment restrains the tumor growth after radiation, we injected 5×10^4 LLC cells in a volume of 50µL subcutaneously in the lower limbs of $Asm^{-/-}$, tAsm and wt mice. After 13 days of implantation, the mice

were divided into two groups, tumor-bearing mice without radiation (bear control tumors) and radiated tumor-bearing mice. Radiation with a single dose of 15 Gy was limited to tumors in the right limbs (primary tumors) and did not extend to tumors in the left limbs, which were preserved from radiation via a shelter (secondary tumors). Tumor sizes were (80±30) mm^3 on day 0 (day of radiation) which is also day 13 post implantation. Tumors were measured every other day with a digital caliper and the volume was determined according to the formula [(L×W×H)/2]. Tumor fold, which is the ratio of tumor volume at the respective time point to the tumor volume at the day of radiation and represents the tumor growth, was compared between the different genotypes. The comparison showed that when no radiation was performed, tumors in $Asm^{-/-}$ mice had a more rapid growth compared to wt and tAsm mice (Figure. 10 A); however, radiated tumors in wt, tAsm and $Asm^{-/-}$ mice showed no difference in their growth. (Figure.10 B). These data demonstrate the ability of radiation to control the development of the tumors regardless of the expression of Asm.

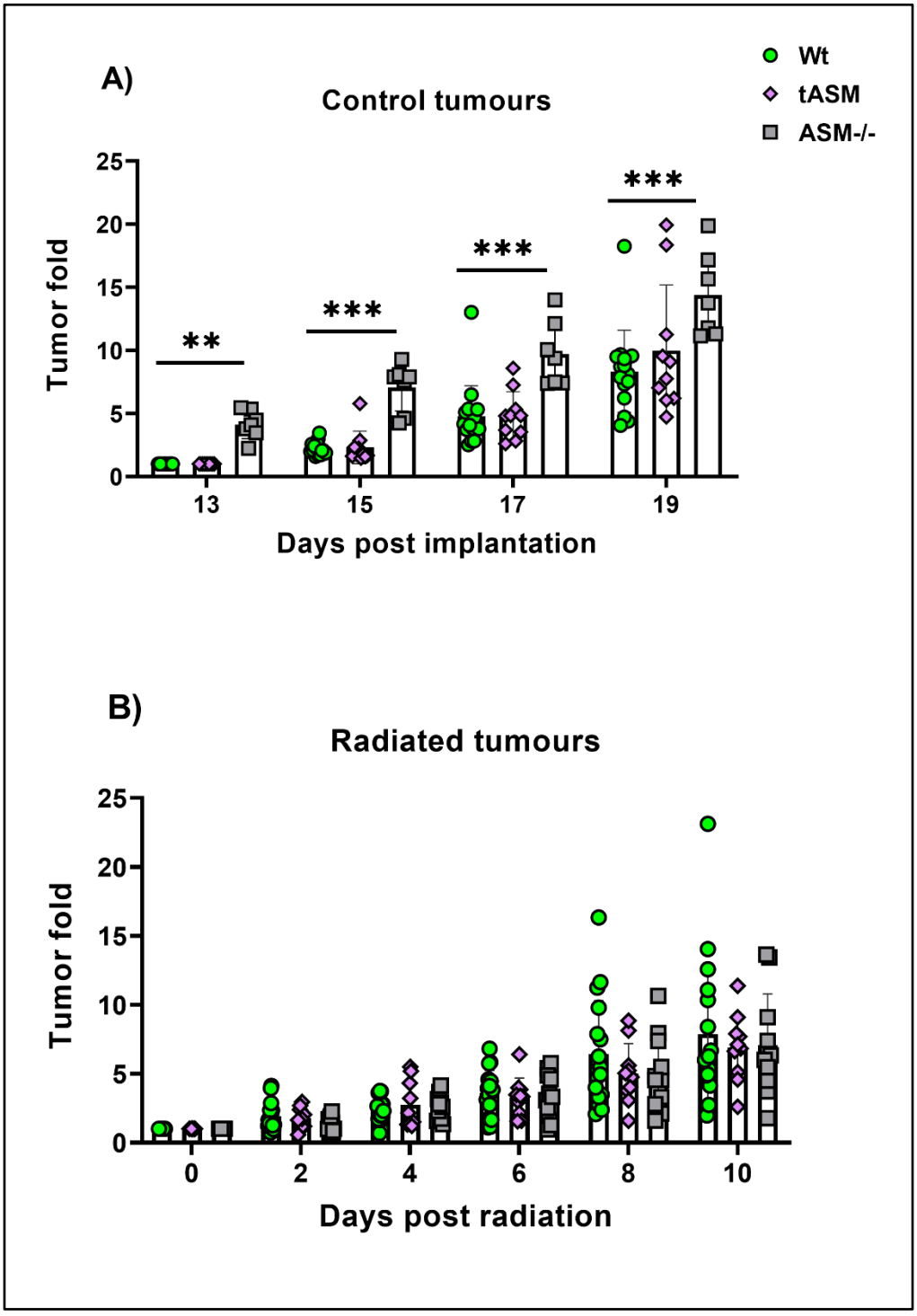

Figure 10. Effect of radiation on tumor growth

(A)Control tumors in mice left without radiation. (B) Primary tumors in the radiated mice. 5×10^4 LLC cells in 25 µL along with 25 µL Matrigel were inoculated subcutaneously in the right and left lower limbs. Tumor sizes were calculated by the following equation[(L×W×H)/2] every other day. In radiated mice, tumors in the right lower limbs were radiated when they reached (80 ±30) mm^3 with a single dose of 15 Gy (primary tumors), whereas tumors in the left lower limb were not radiated (secondary tumors).

Displayed is the tumor fold, which represents the ratio of the tumor volume at the respective time point to the tumor volume on the day of radiation (day 0) in radiated mice or day 13 (post implantation) in mice without radiation. Statistical significance between the three genotypes was determined by analysis of variance (two-way ANOVA) followed by Bonferroni's selected comparisons test. P-values ($p \leq 0.01$, $p \leq 0.001$) are indicated by an asterisk** or ***, respectively. n (control group): wt=16, tAsm=11, $Asm^{-/-}$=7, n (radiated group): wt=18, tAsm=11, $Asm^{-/-}$ =11.

3.3 Overexpression of Asm in recipient mice enhances abscopal effect

To determine whether the expression of Asm has an impact on the abscopal anti-tumor effect after irradiation, LLC cells were injected subcutaneously in both lower limbs. The mice were divided into a control group, as their tumors were left without radiation, and a radiated group. Only tumors in the right limbs were radiated (primary tumor) in the radiated mice, while a shelter covered the entire body, including tumors in the left limbs (secondary tumor). Although the growth of the secondary tumors in $Asm^{-/-}$ mice, wt mice showed a tendency to delayed growth. Only in tAsm mice we found a significant reduction of tumor growth in secondary tumors, which represents a measurable abscopal effect (Figure.11). In contrast, the primary tumors were equally sensitive to the radiation irrespective of the Asm expression/ genotype.

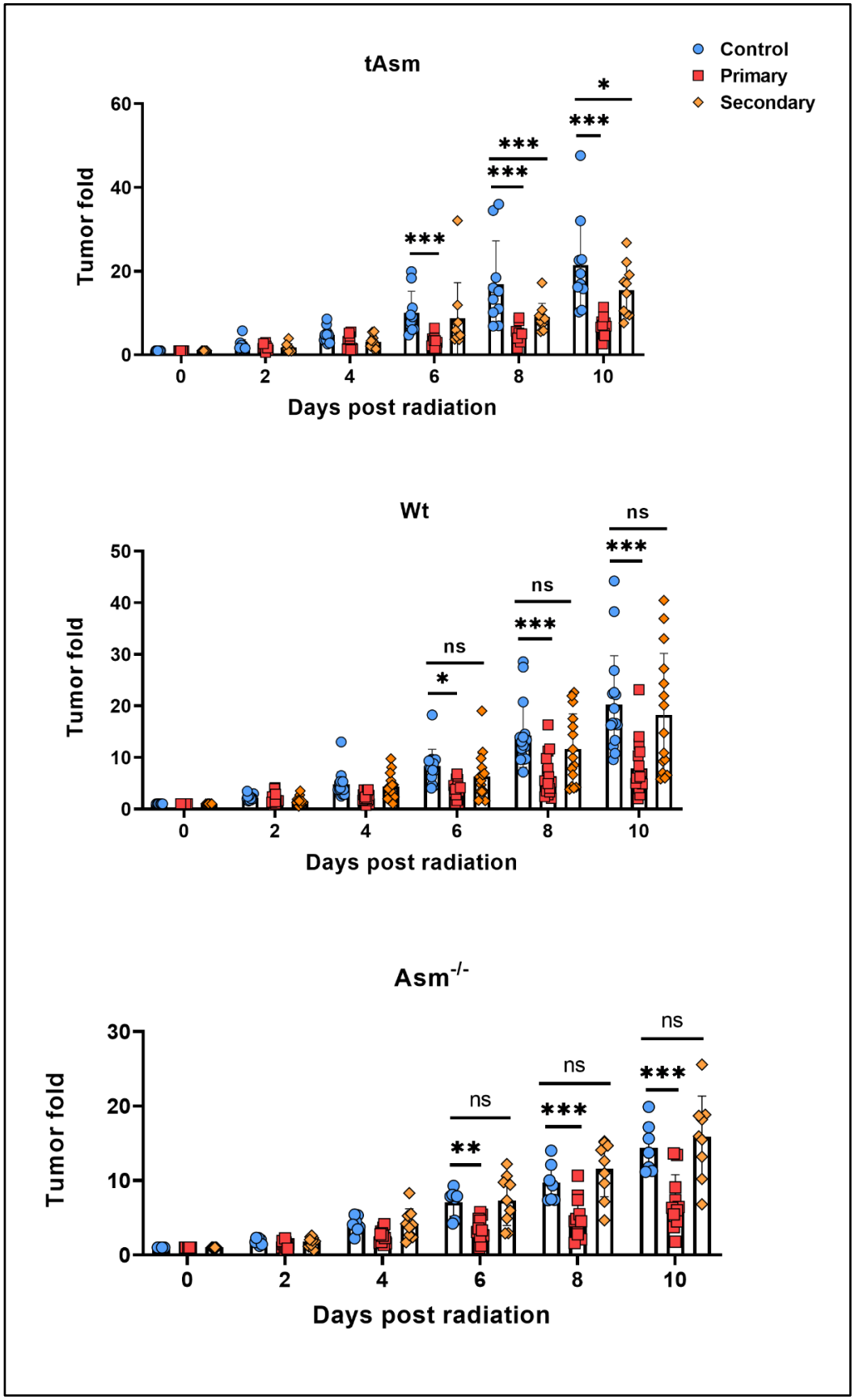
tAsm
Control
Primary
Secondary
Tumor fold
Days post radiation
***
***
***
*
Wt
Tumor fold
Days post radiation
*
ns
***
ns
***
ns
Asm-/-
Tumor fold
Days post radiation
**
ns
***
ns
***
ns

Figure 11. Tumor growth in different genotypes

5×10^4 LLC cells /25 µL along with 25 µL Matrigel were inoculated subcutaneously in the right and left lower limbs. Tumors were measured every other day by a digital caliper, and the volume was calculated by the following equation[(L×W×H)/2]. Tumors in the right lower limbs were radiated when they reached (80 ±30) mm^3 with a single dose of 15 Gy (primary tumors), whereas tumors in the left lower limb were not radiated (secondary tumors). Tumors in $Asm^{-/-}$ mice were characterized by faster growth than wt and tAsm mice and were radiated on day 11 post-implantation. Tumors in wt and tAsm were radiated on day 13 post-implantation. Displayed is the tumor fold, representing the ratio of the tumor volume at the respective time point to the tumor volume on the day of radiation (day 0), which is, for control littermates, day 13 post-implantation in wt and tAsm mice or day 11 post-implantations in $Asm^{-/-}$ mice. Statistical significance between control, primary and secondary tumors was determined by analysis of variance (two-way ANOVA) followed by Bonferroni's selected comparisons test. P-values ($p\leq0.05$, $p\leq0.01$, $p\leq0.001$) are indicated by an asterisk * or ** or ***, respectively. N (wt group): control=16, primary=11, secondary=17 / n (tAsm group): control=11, primary=11, secondary =11 / n ($Asm^{-/-}$ group): control=7, primary=11, secondary =10.

3.4 Asm deficiency prompts the creation of immune suppressor cells in the tumor microenvironment, and the overexpression of Asm enhances recruitment of APCs

Radiation restrains tumor outgrowth by inducing apoptosis and releasing tumor antigens, which trigger an immune response against the radiated tumor. The infiltrated WBCs, i.e., APCs, NK cells and T-cells, enhances tumor cytotoxicity and prompt a systemic immune response against the same antigens in the distant parts (Demaria et al., 2004). Therefore, we investigated the infiltration of WBCs in tumors of non-radiated mice (control tumors) or in primary and secondary tumors, where the primary tumor were irradiated with a single dose of 15 Gy (Figure. 12) in the three genotypes. In the first group of experiments, we analysed mice/tumors at day 10 after irradiation. We found an infiltration of neutrophils, DCs and monocytes in $Asm^{-/-}$ mice control tumors. Further, in primary and secondary, we found a higher infiltration of macrophages, NK cells, DCs and Tregs in $Asm^{-/-}$ mice. As no significant difference in CTLs, which were suggested to be the crucial cells in anti-tumor effect after radiation, was found after 10 days of radiation, we decided to analyse mice/tumors after 4 days in a second set of experiments. Moreover, most of the recruited macrophages in $Asm^{-/-}$ mice were suspected to be TAMs; consequently, intracellular staining for IL-10 was conducted to differentiate the APCs from TAMs and

MDSCs. Nevertheless, no difference was noted in T-cells recruitment; more PMN-MDSC and intermediate monocytes in untreated tumors of $Asm^{-/-}$ and tAsm mice were detected, respectively. Furthermore, enhanced intermediate monocytes and DCs recruitment in tAsm mice along with higher creation of TAMs and Tregs in $Asm^{-/-}$ mice, were found in both primary and secondary tumors (Figure. 13).

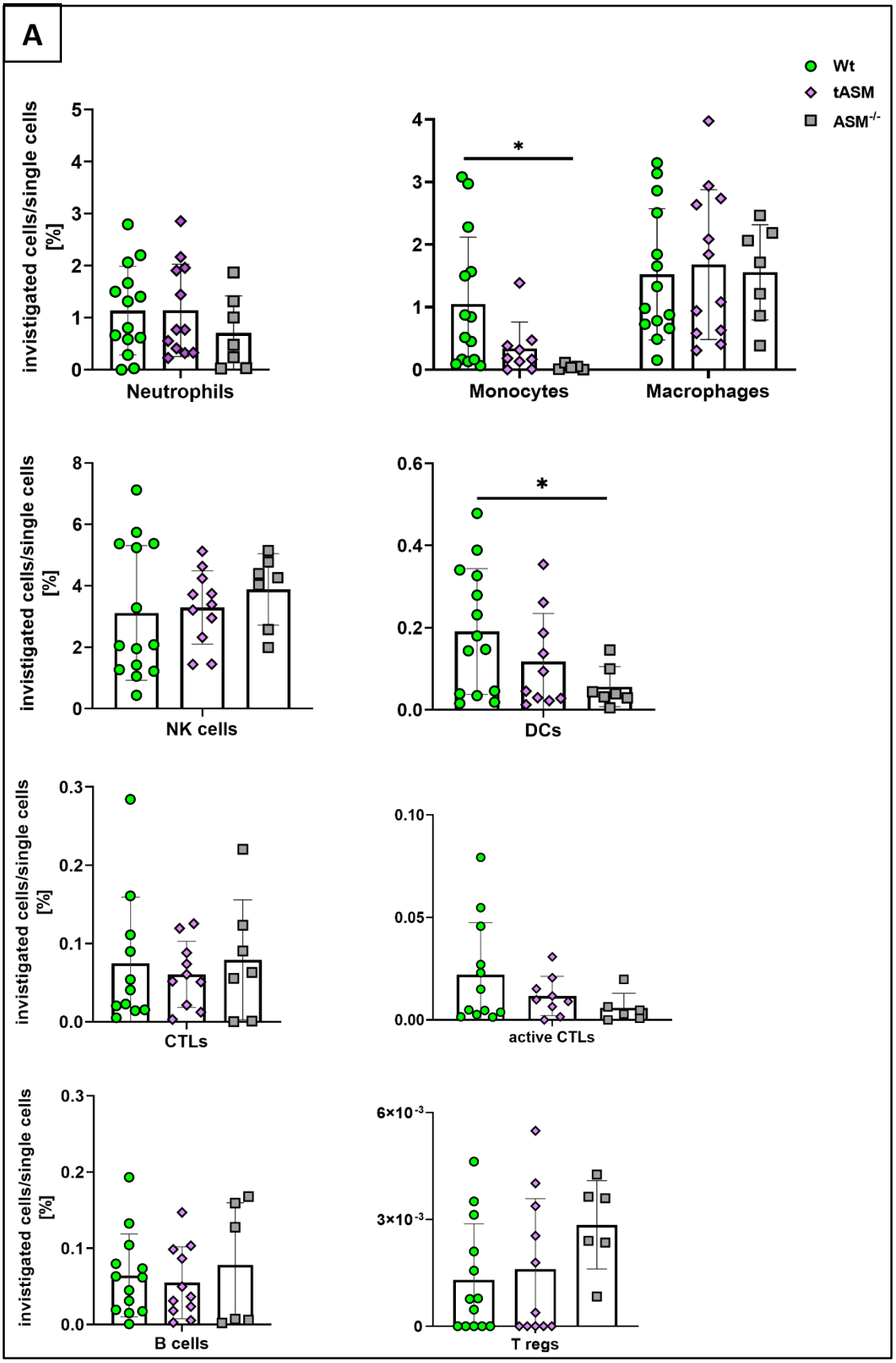
A
Wt
tASM
ASM-/-
invistigated cells/single cells [%]
Neutrophils
Monocytes
Macrophages
NK cells
DCs
CTLs
active CTLs
B cells
T regs
*
*

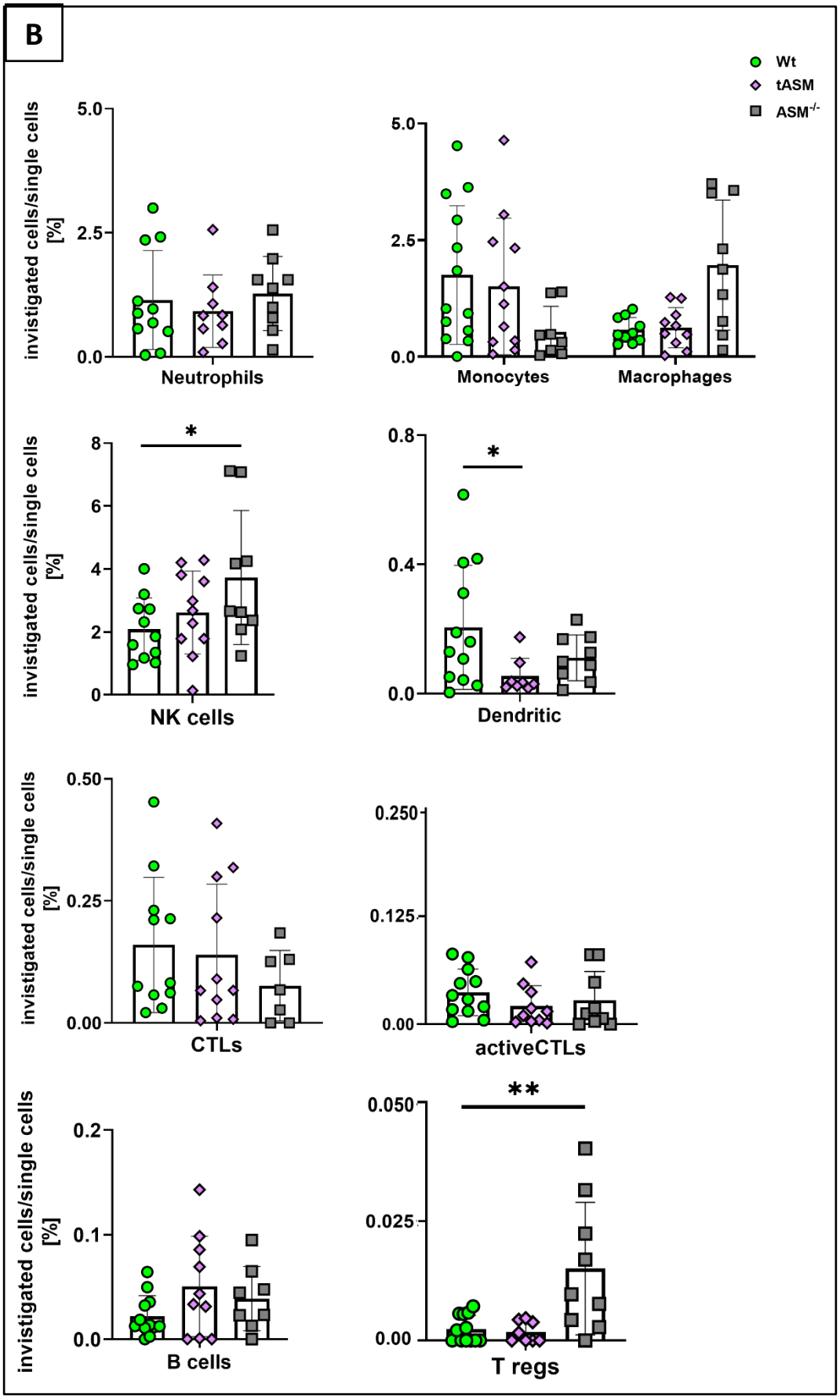
B
Wt
tASM
ASM-/-
invistigated cells/single cells [%]
Neutrophils
Monocytes
Macrophages
NK cells
Dendritic
CTLs
activeCTLs
B cells
T regs
*
*
**

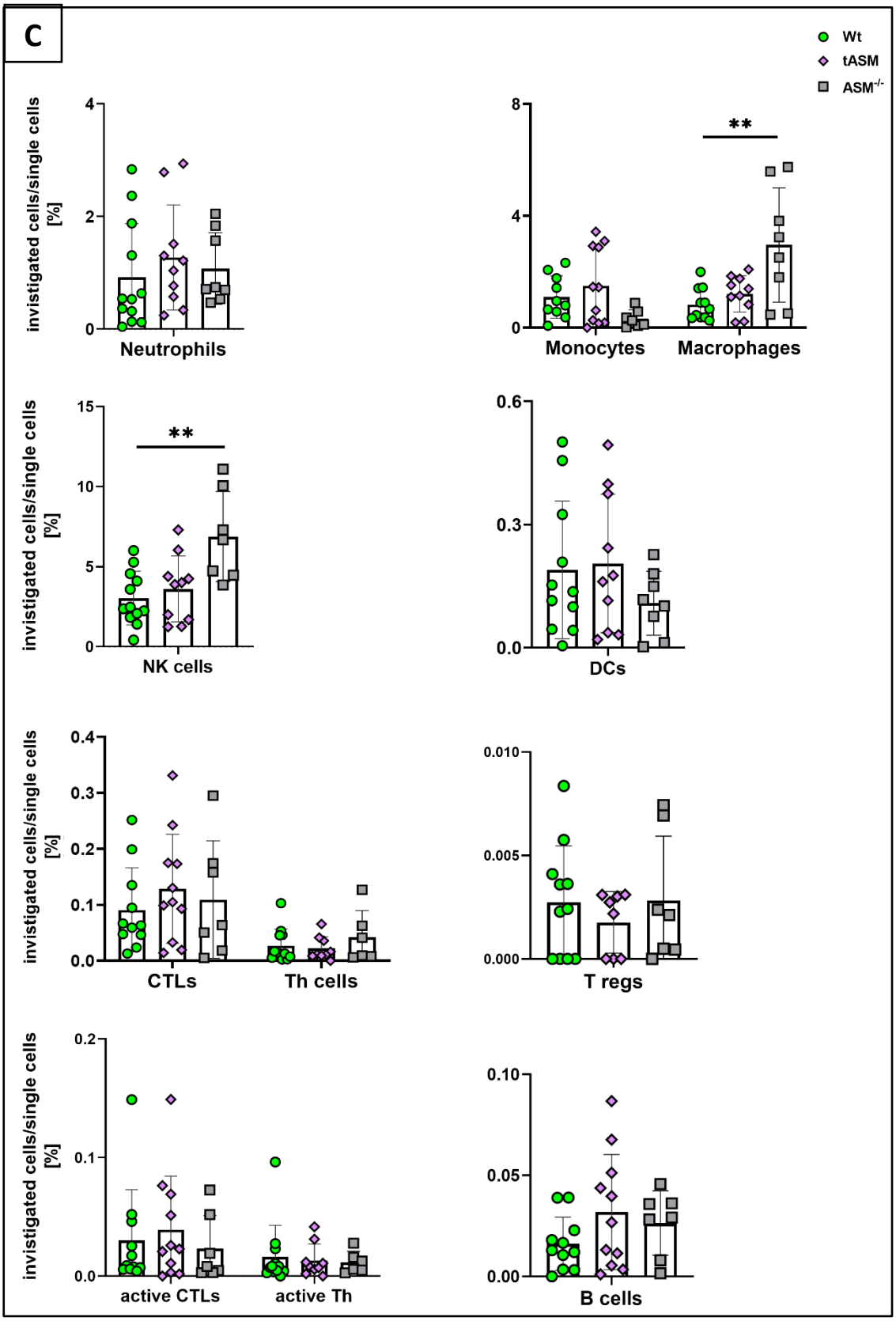

Figure 12. Infiltration in tumors after 10 days of radiation

A)- Infiltration in control tumors, B)- primary tumors, C)- secondary tumors. Mice were sacrificed 10 days after irradiation, and tumors were extracted to analyse the infiltrating immune cells by flow cytometry. After obtaining a single-cell suspension and respective immune staining, absolute numbers were quantified to 1g of tumor mass, and percentages were calculated in relation to total cell number. Statistical analysis between the genotypes was determined by analysis of variance (one-way ANOVA) followed by Bonferroni's selected comparisons test. P-values ($p \leq 0.05$, $p \leq 0.01$) are indicated by an asterisk * or **, respectively. Outliers were excluded according to GraphPad statistical analysis. n: Wt =13, tAsm= 10, $Asm^{-/-}$ =7.

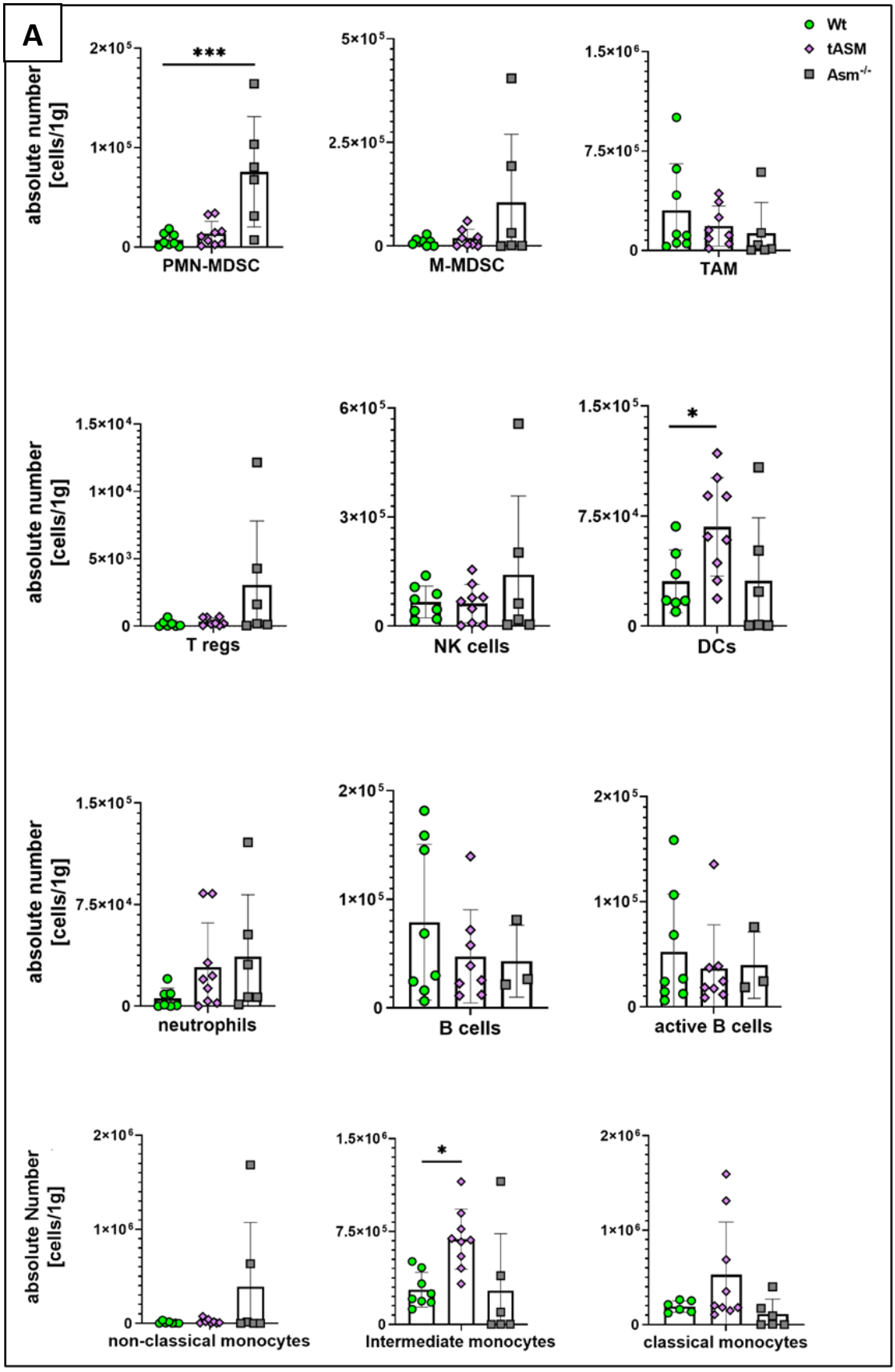
A
Wt
tASM
Asm-/-
absolute number [cells/1g]
PMN-MDSC
M-MDSC
TAM
T regs
NK cells
DCs
neutrophils
B cells
active B cells
absolute Number [cells/1g]
non-classical monocytes
Intermediate monocytes
classical monocytes
***
*
*

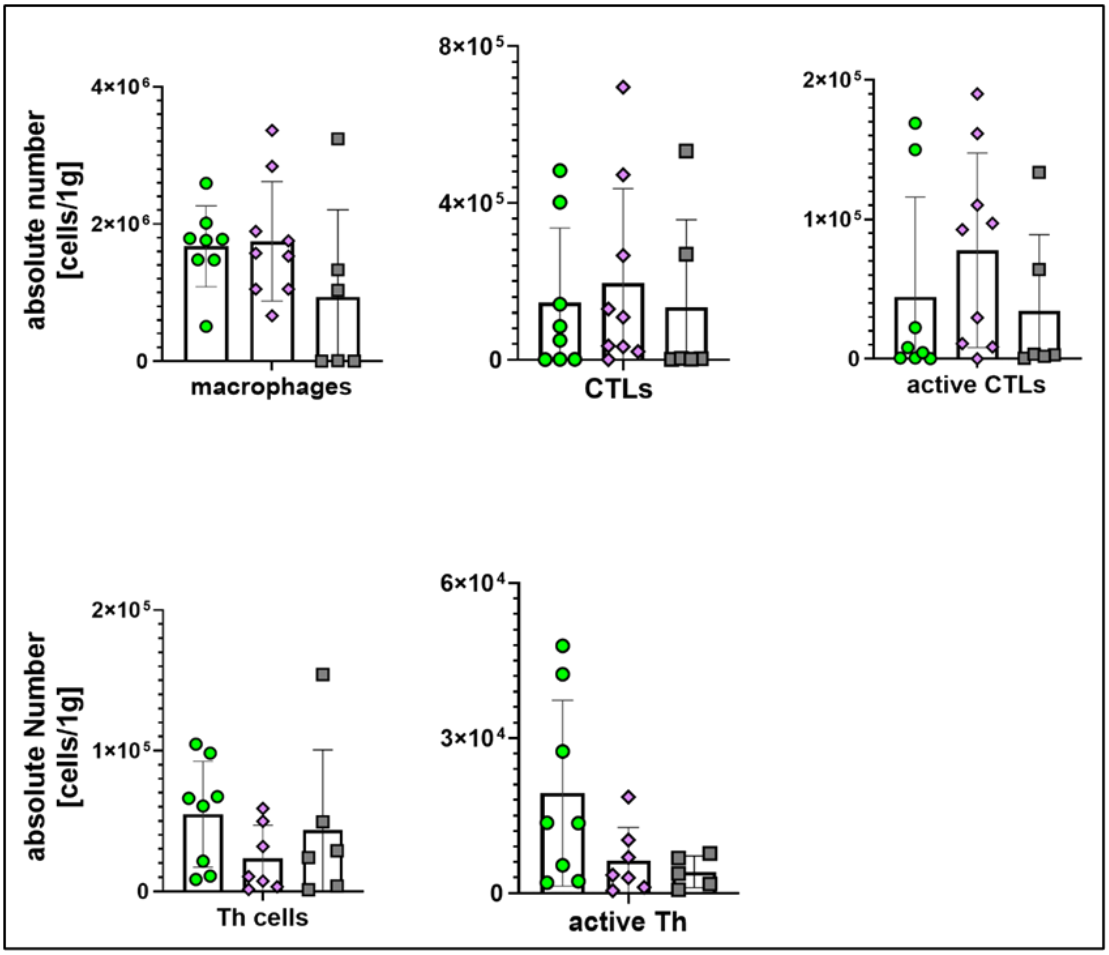
absolute number [cells/1g]
4×10⁶
2×10⁶
0
macrophages
8×10⁵
4×10⁵
0
CTLs
2×10⁵
1×10⁵
0
active CTLs
absolute Number [cells/1g]
2×10⁵
1×10⁵
0
Th cells
6×10⁴
3×10⁴
0
active Th

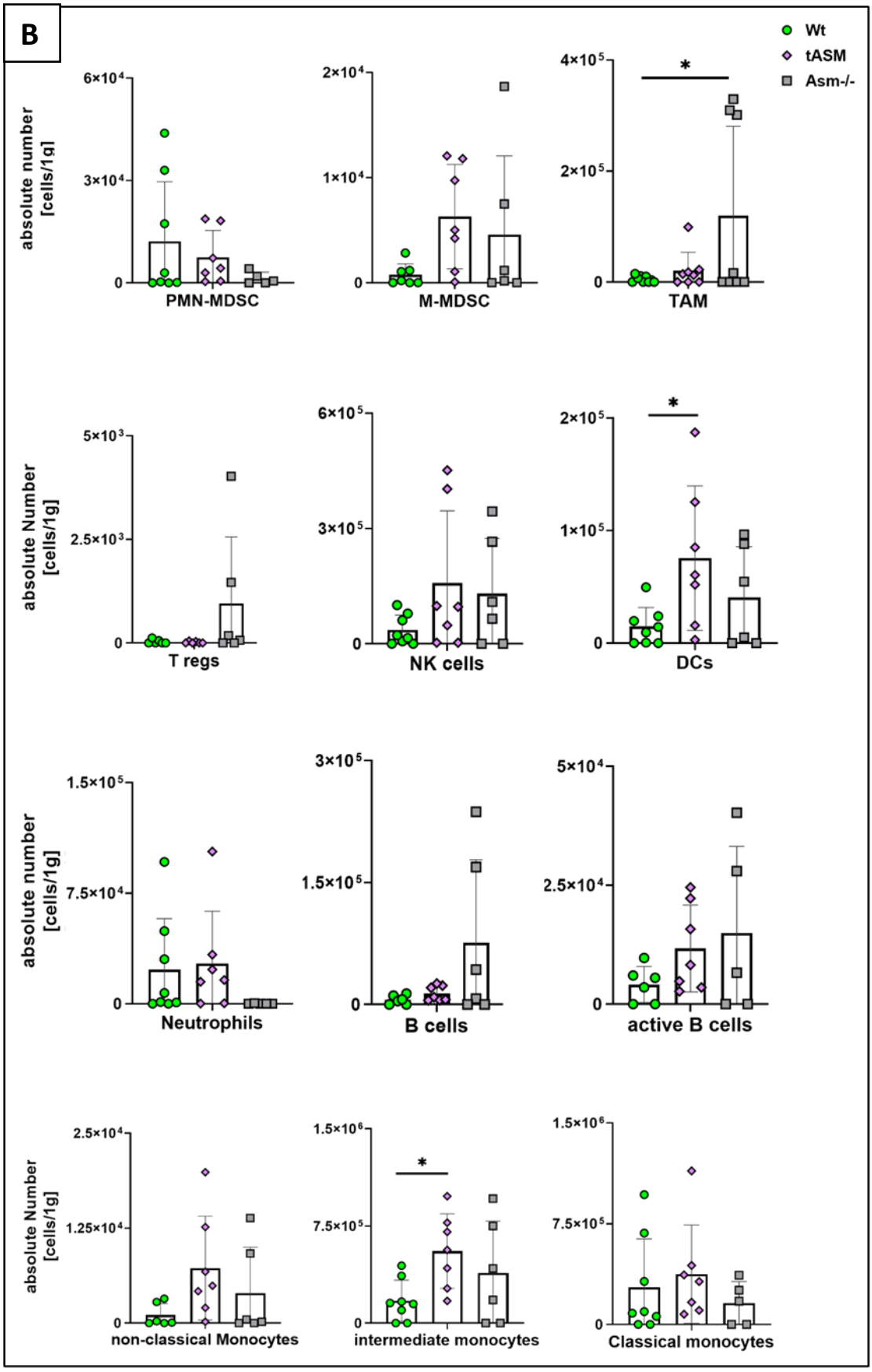
B
Wt
tASM
Asm-/-
absolute number [cells/1g]
6×10⁴
3×10⁴
0
PMN-MDSC
2×10⁴
1×10⁴
0
M-MDSC
4×10⁵
2×10⁵
0
*
TAM
absolute Number [cells/1g]
5×10³
2.5×10³
0
T regs
6×10⁵
3×10⁵
0
NK cells
2×10⁵
1×10⁵
0
*
DCs
absolute number [cells/1g]
1.5×10⁵
7.5×10⁴
0
Neutrophils
3×10⁵
1.5×10⁵
0
B cells
5×10⁴
2.5×10⁴
0
active B cells
absolute Number [cells/1g]
2.5×10⁴
1.25×10⁴
0
non-classical Monocytes
1.5×10⁶
7.5×10⁵
0
*
intermediate monocytes
1.5×10⁶
7.5×10⁵
0
Classical monocytes

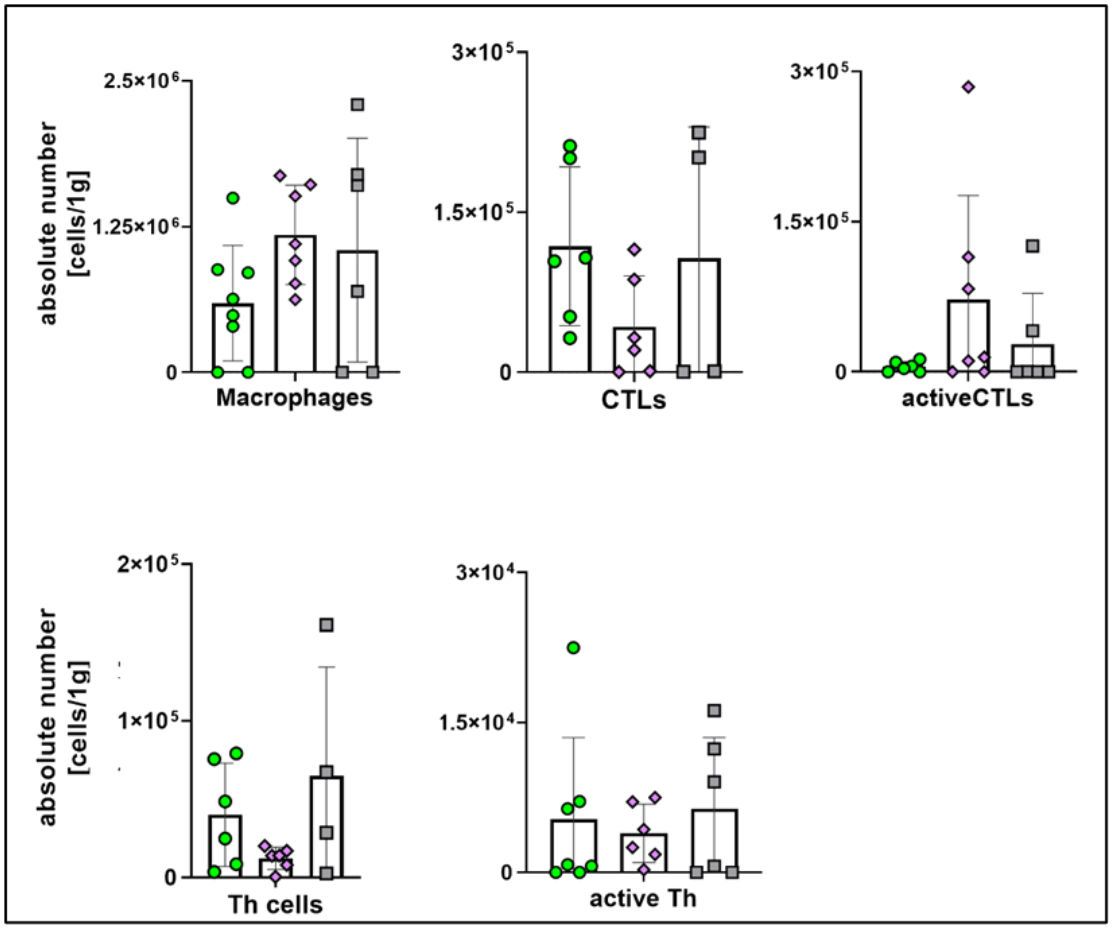
absolute number [cells/1g]
2.5×10⁶
1.25×10⁶
0
Macrophages
3×10⁵
1.5×10⁵
0
CTLs
3×10⁵
1.5×10⁵
0
activeCTLs
absolute number [cells/1g]
2×10⁵
1×10⁵
0
Th cells
3×10⁴
1.5×10⁴
0
active Th

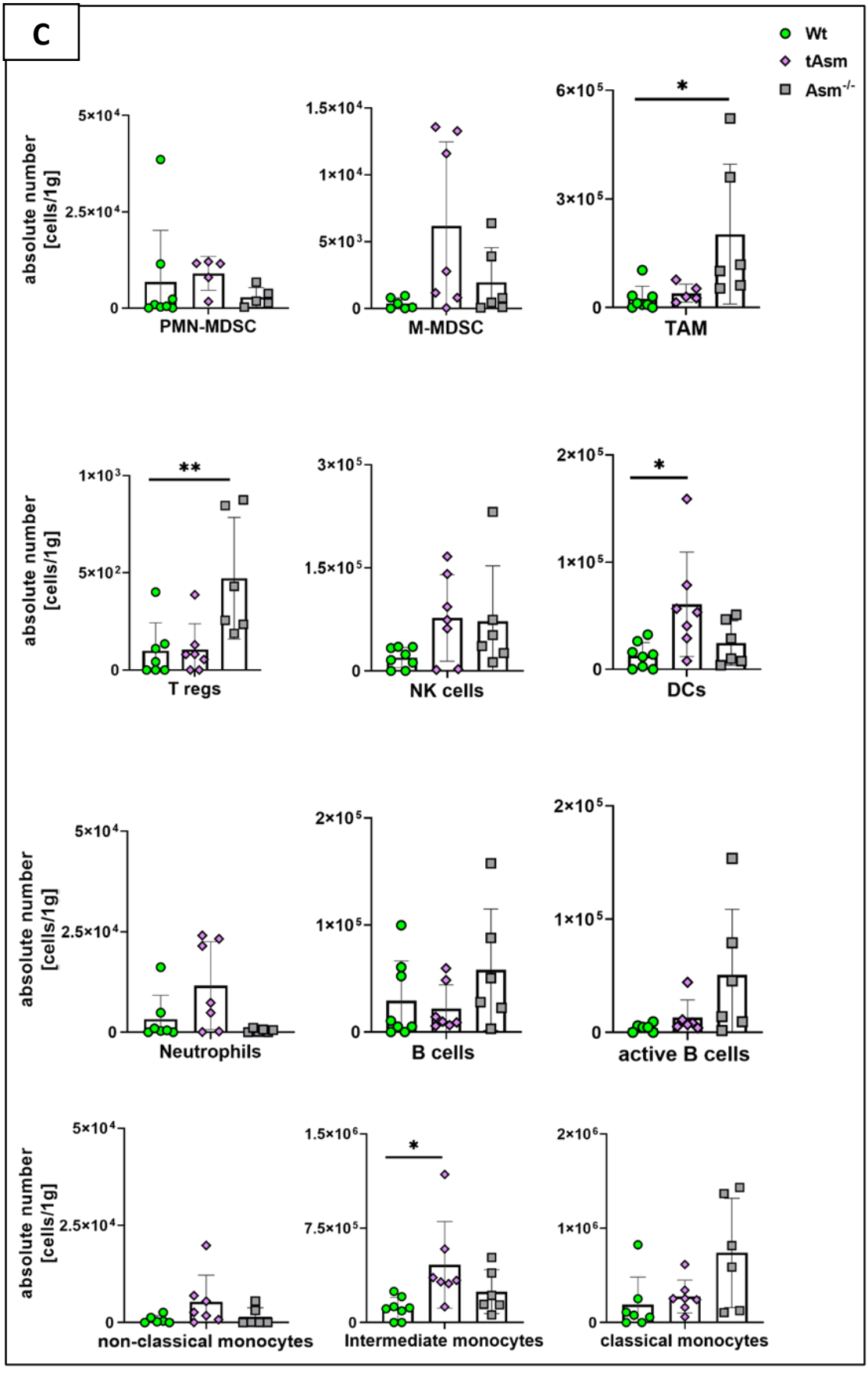
C
Wt
tAsm
Asm-/-
absolute number [cells/1g]
PMN-MDSC
M-MDSC
TAM
T regs
NK cells
DCs
Neutrophils
B cells
active B cells
non-classical monocytes
Intermediate monocytes
classical monocytes
*
**

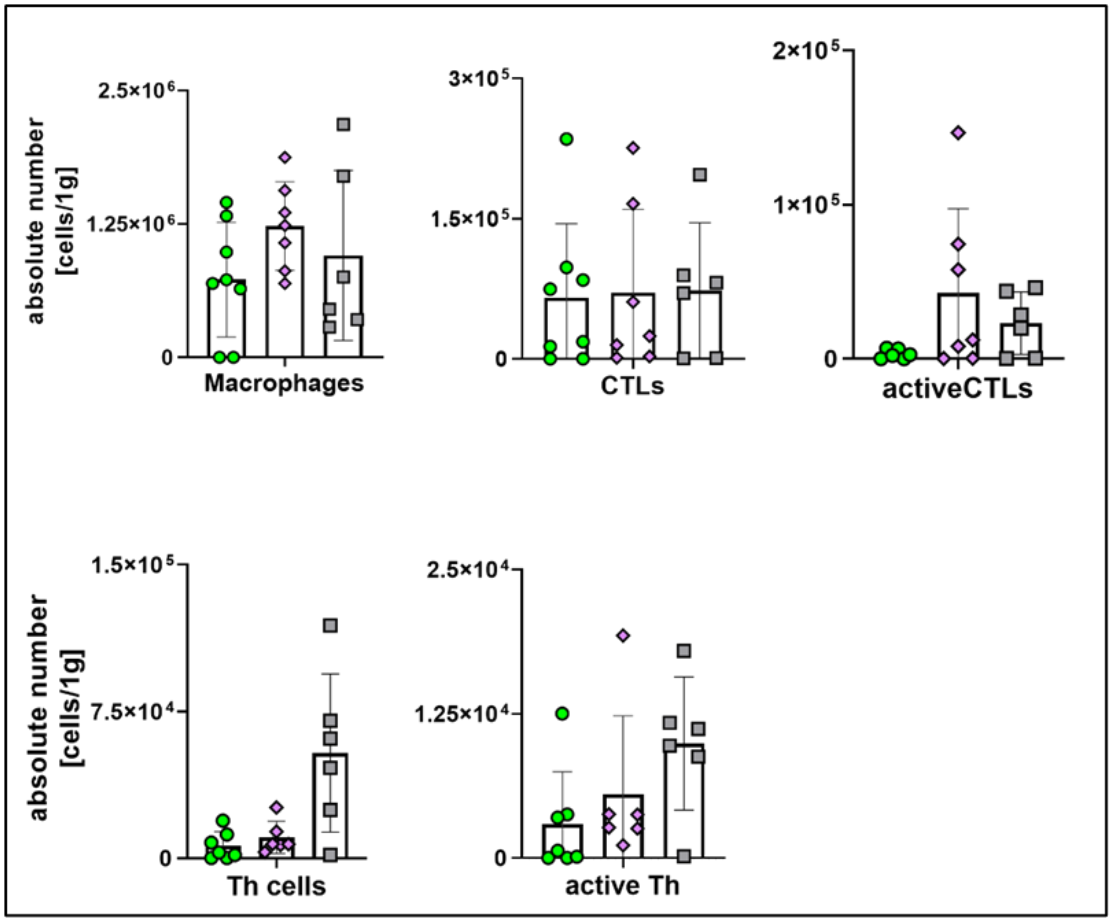

Figure 13. Infiltration in tumors 4 days after radiation

(A) Infiltration in control tumors, (B) primary tumors and (C) secondary tumors. Mice were sacrificed 4 days after irradiation and tumors were extracted to analyse the infiltrating immune cells by flow cytometry after obtaining a single-cell suspension and respective immune staining. Absolute numbers were quantified to 1g of tumor mass. Statistical analysis between the genotypes was determined by analysis of variance (one-way ANOVA) followed by Bonferroni's selected comparisons test. P-values ($p \leq 0.05$, $p \leq 0.01$, $p \leq 0{,}001$) are indicated by an asterisk * or ** or *** respectively. Outliers were excluded according to GraphPad statistical analysis. n: wt =8, tAsm= 7, $Asm^{-/-}$ =6.

3.5 Sequestration of neutrophils and DCs after radiation in the spleen in Asm deficient mice

The spleen is the largest secondary lymphoid organ in the body and hosts a wide range of immunologic functions alongside its roles in haematopoiesis and red blood cell clearance. After 10 days of radiation, no difference in CTLs percentage was detected between the studied genotypes. Still, a higher percentage of Tregs and macrophages were found in the spleen of non-radiated and radiated $Asm^{-/-}$ mice, while the neutrophils were higher solely after radiation in $Asm^{-/-}$ mice (Figure. 14). Analysis of spleens after 4 days of radiation also exhibited no difference in T-cell proliferation in the untreated or treated mice. Yet, an increase in monocyte numbers together with B-cell proliferation and activation in tAsm mice, as well as a decline in B cells in $Asm^{-/-}$ mice, was observed in the non-radiated mice (Figure.4.5.2). Additionally, an accumulation of neutrophils, DCs and Tregs in $Asm^{-/-}$ mice was witnessed after radiation (Figure. 15).

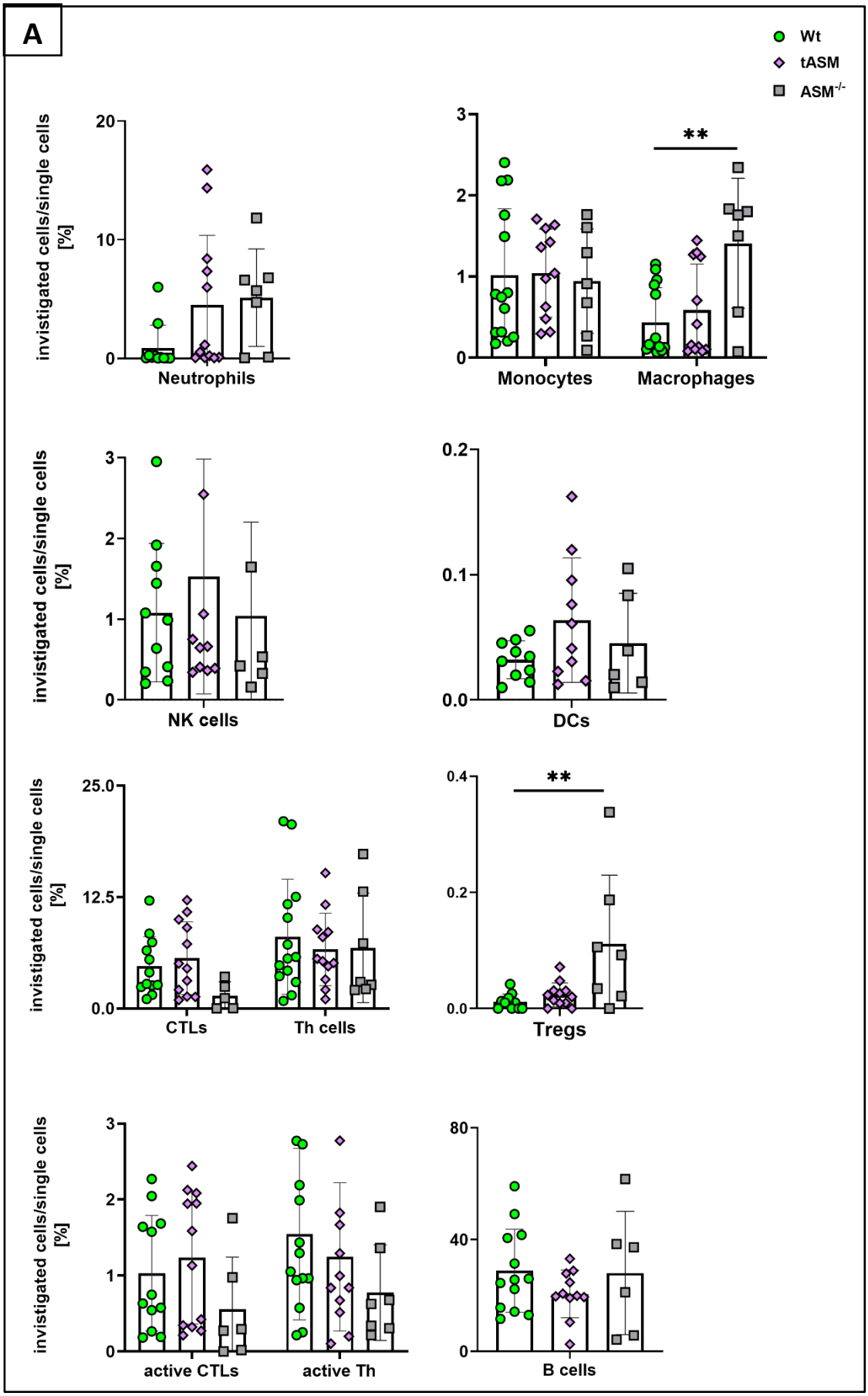
A
Wt
tASM
ASM-/-
invistigated cells/single cells [%]
Neutrophils
Monocytes
Macrophages
**
NK cells
DCs
CTLs
Th cells
Tregs
**
active CTLs
active Th
B cells

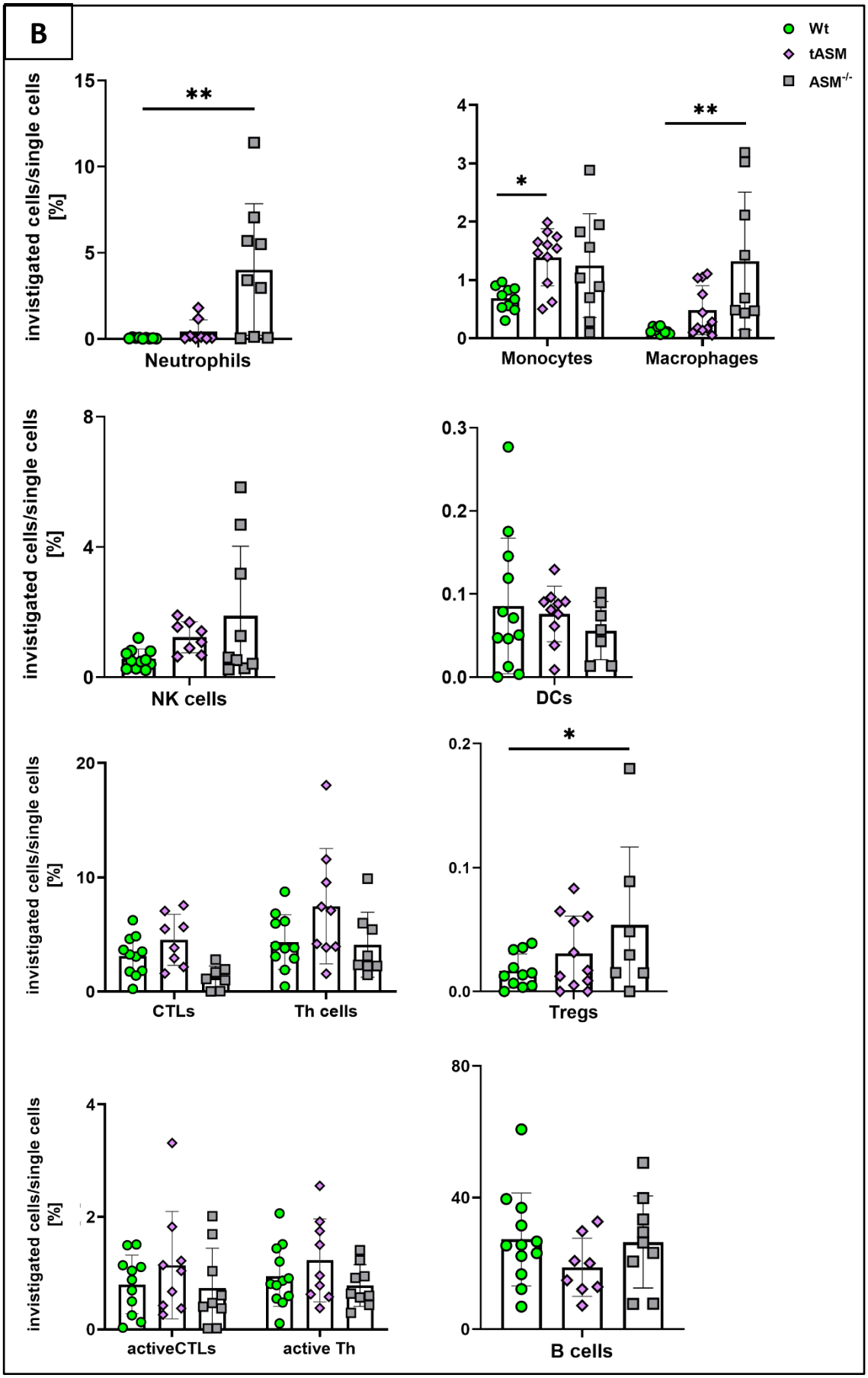
B
Wt
tASM
ASM-/-
invistigated cells/single cells [%]
Neutrophils
Monocytes
Macrophages
NK cells
DCs
CTLs
Th cells
Tregs
activeCTLs
active Th
B cells

Figure 14. WBCs in spleen 10 days after radiation

A) WBCs in spleen of control mice and B) in radiated mice. Mice were sacrificed 10 days after radiation and spleens were harvested to analyse their immune cells in the flow cytometry. Single-cell suspensions were obtained and cells were incubated with respective conjugated antibodies. The percentage was calculated according to [(subtype cells numbers/single cells number) ×100]. Statistical significance between the three genotypes was determined by analysis of variance (one-way ANOVA) followed by Bonferroni's selected comparisons test. P-values ($p \leq 0.05$, $p \leq 0.01$) are indicated by an asterisk * or **, respectively. Outliers were excluded according to GraphPad statistical analyze. n: wt =11, tAsm= 10, $Asm^{-/-}$ =9.

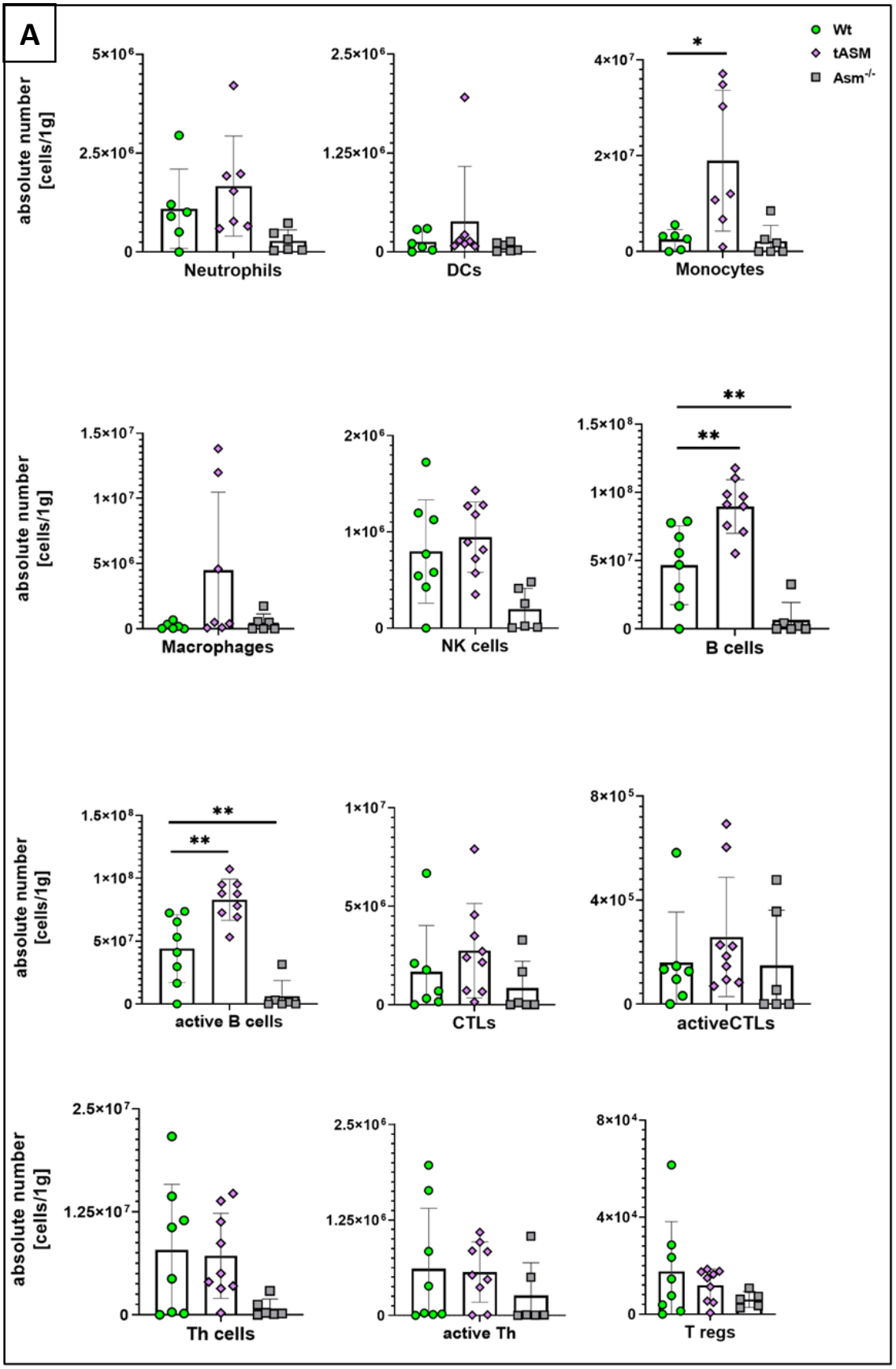
A
Wt
tASM
Asm-/-
absolute number [cells/1g]
Neutrophils
DCs
Monocytes
Macrophages
NK cells
B cells
active B cells
CTLs
activeCTLs
Th cells
active Th
T regs
*
**
**

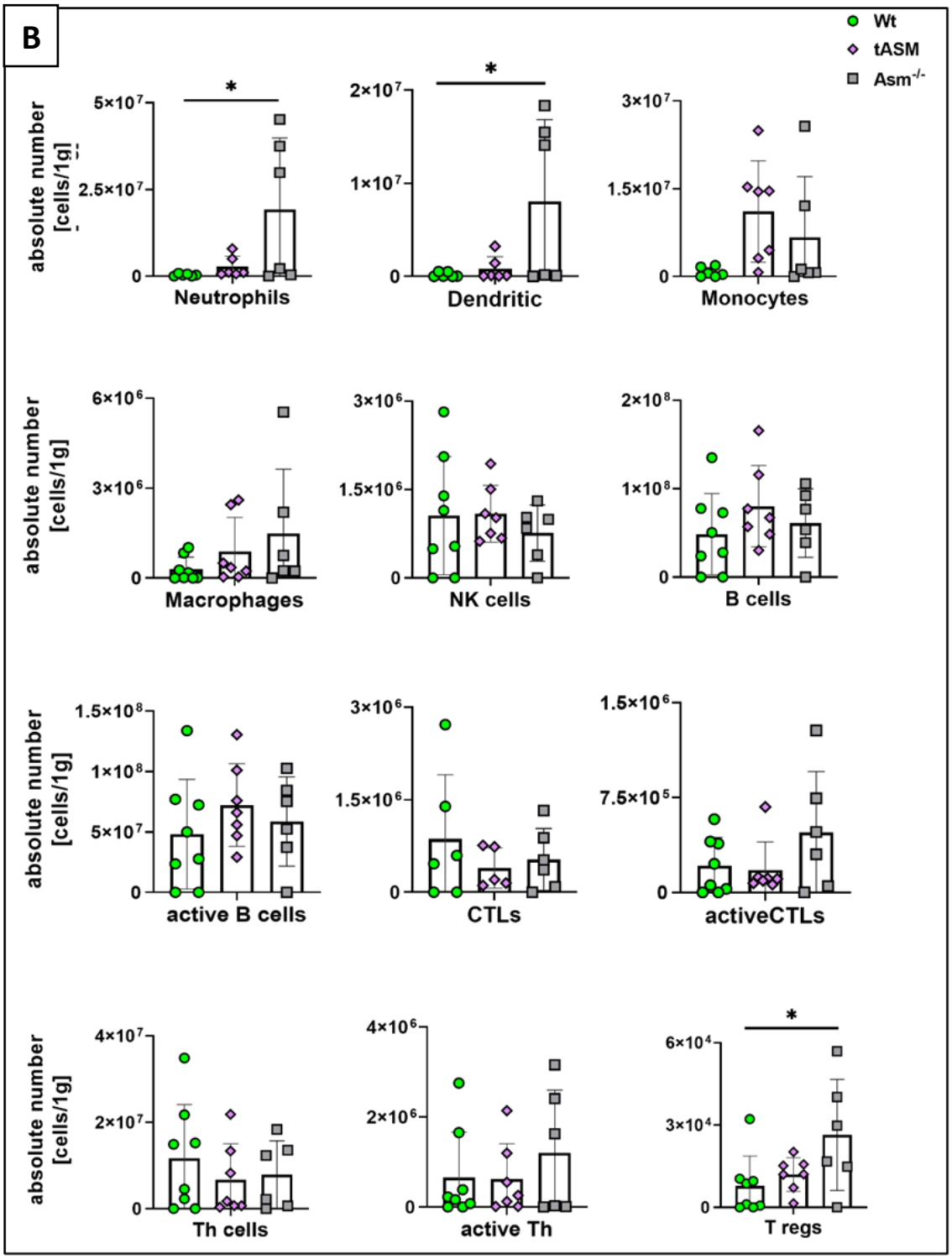

Figure 15. WBCs in Spleen 4 days after radiation

A) WBCs in spleen of control mice and B) in radiated mice. Mice were sacrificed 4 days after radiation, and spleens were harvested to analyse their immune cells in the flow cytometry. Single-cell suspensions were obtained and cells were incubated with respective conjugated antibodies. Absolute numbers were quantified to 1g of spleen mass. Statistical analysis between the genotypes was determined by analysis of variance

(one-way ANOVA) followed by Bonferroni's selected comparisons test. P-values ($p \leq 0.05$, $p \leq 0.01$) are indicated by an asterisk * or **, respectively. Outliers were excluded according to GraphPad statistical analyse. n: wt =8, tAsm= 6, $Asm^{-/-}$ =6.

3.6 Asm enhances cross-presenting antigens and proliferation of CTLs in inguinal LN after radiation

Sentinel inguinal lymph nodes include B and T-cells and are responsible for filtering the lymph from the lower limbs. To see if they were involved in the witnessed abscopal effect in tAsm mice, we analysed inguinal lymph nodes regarding their immune cell content. After 10 days of radiation, right and left inguinal lymph nodes were extracted from the non-radiated (control LNs) and radiated mice. Single-cell suspensions were prepared after mixing the lymph nodes from both sides. In non-radiated mice, macrophage numbers were higher in tAsm mice, whereas CTLs numbers were less in $Asm^{-/-}$ mice. With radiation, the analysis of inguinal lymph nodes showed not only more NK cells and CTLs, but also a lowering in Treg numbers in tAsm mice; moreover, DCs, monocytes and B cells were less in $Asm^{-/-}$ mice (Figure. 16). After 4 days of radiation, single-cell suspensions were prepared via control lymph nodes from non-radiated mice or the right (radiated side) and left (non-radiated side) inguinal lymph nodes separately from radiated mice. Control inguinal lymph nodes in $Asm^{-/-}$ were characterized by lower numbers of monocytes, CTLs and B cells, while right and left nodes displayed more B cells and Tregs in $Asm^{-/-}$ after radiation (Figure. 17).

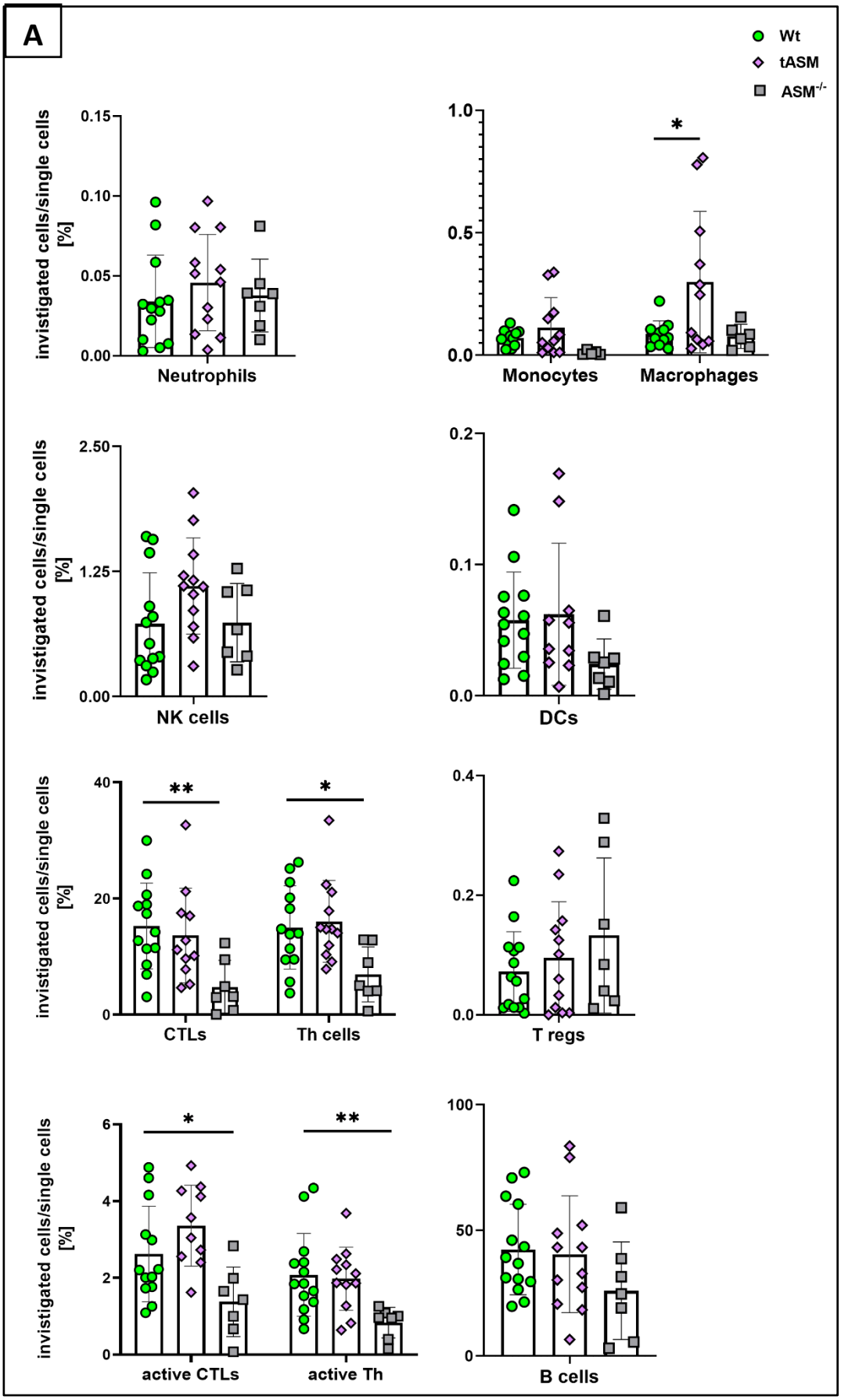
A
Wt
tASM
ASM-/-
invistigated cells/single cells [%]
Neutrophils
Monocytes
Macrophages
NK cells
DCs
CTLs
Th cells
T regs
active CTLs
active Th
B cells
*
**

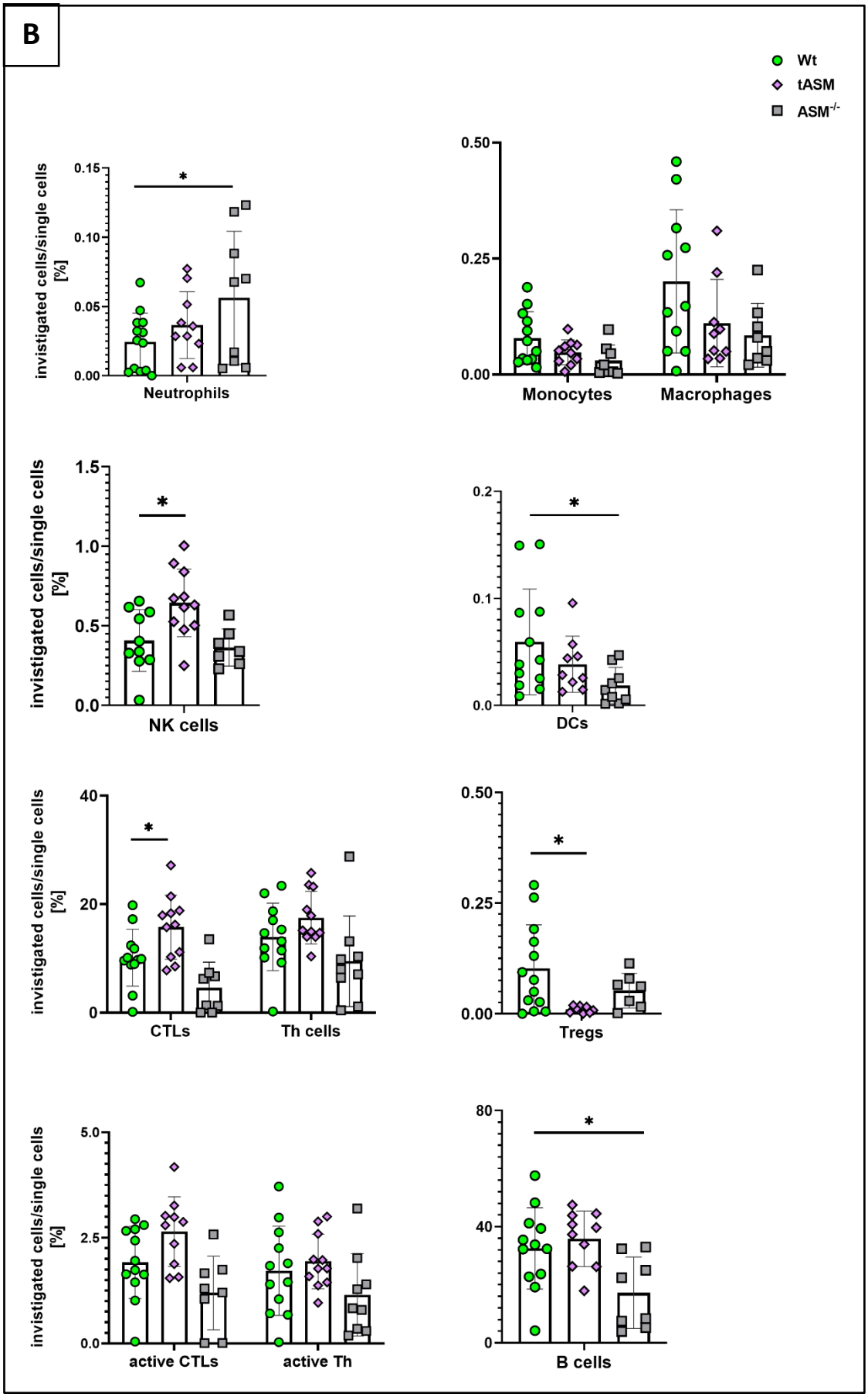
B
Wt
tASM
ASM-/-
invistigated cells/single cells [%]
Neutrophils
Monocytes
Macrophages
NK cells
DCs
CTLs
Th cells
Tregs
active CTLs
active Th
B cells

Figure 16. WBCs in inguinal lymph nodes 10 days after radiation

A) WBCs in control inguinal LN and B) in inguinal LN of radiated mice. Mice were sacrificed 10 days after radiation, and Both right and left inguinal were harvested to analyse their immune cells in the flow cytometry. Single-cell suspensions were obtained and cells were incubated with respective conjugated antibodies. Statistical significance between the three genotypes was determined by analysis of variance (one-way ANOVA) followed by Bonferroni's selected comparisons test. P-values ($p \leq 0.05$, $p \leq 0.01$) are indicated by an asterisk * or **, respectively. Outliers were excluded according to GraphPad statistical analysis. n: wt =11, tAsm= 11, $Asm^{-/-}$ =7.

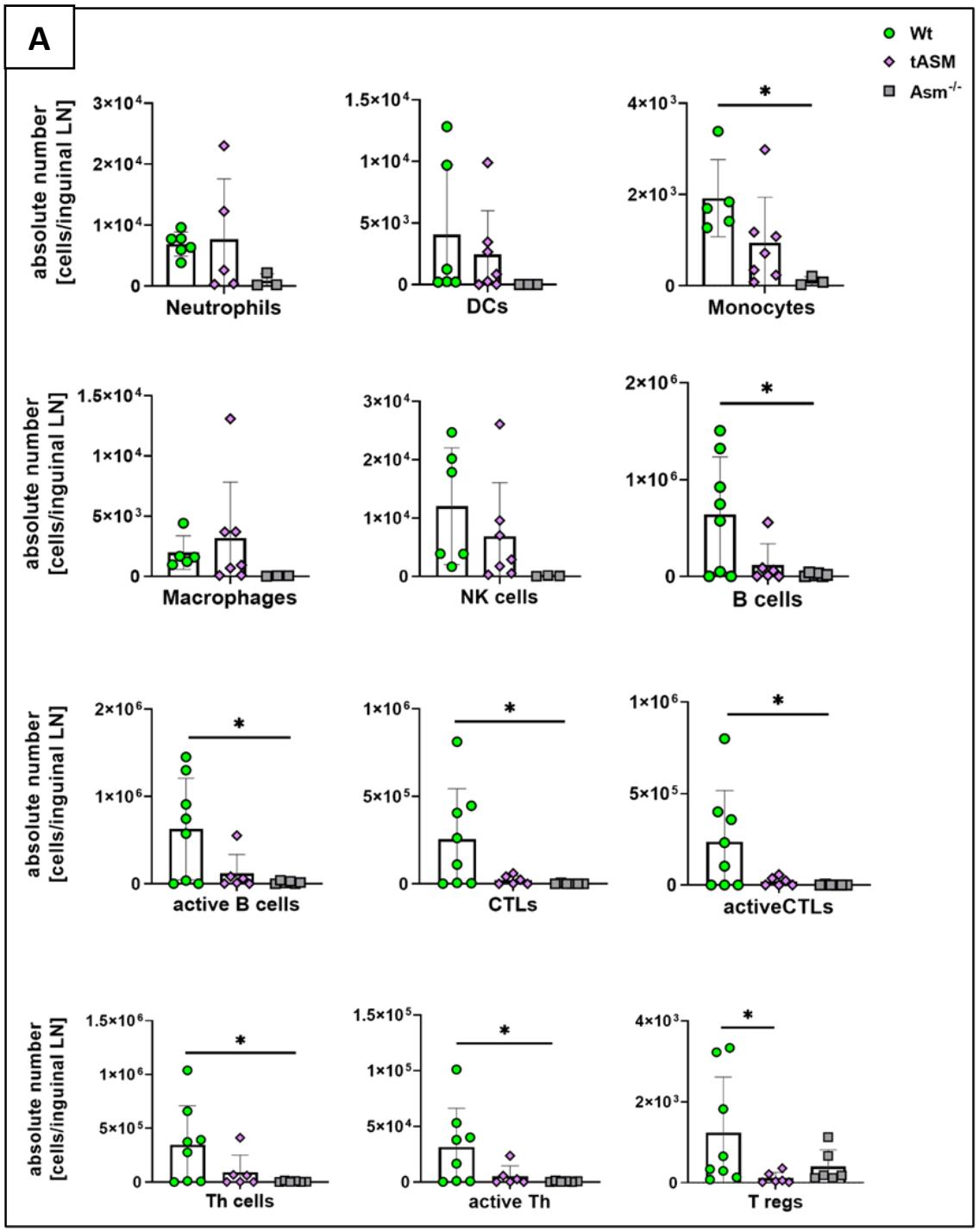
A
Wt
tASM
Asm-/-
absolute number [cells/inguinal LN]
Neutrophils
DCs
Monocytes
Macrophages
NK cells
B cells
active B cells
CTLs
activeCTLs
Th cells
active Th
T regs
*

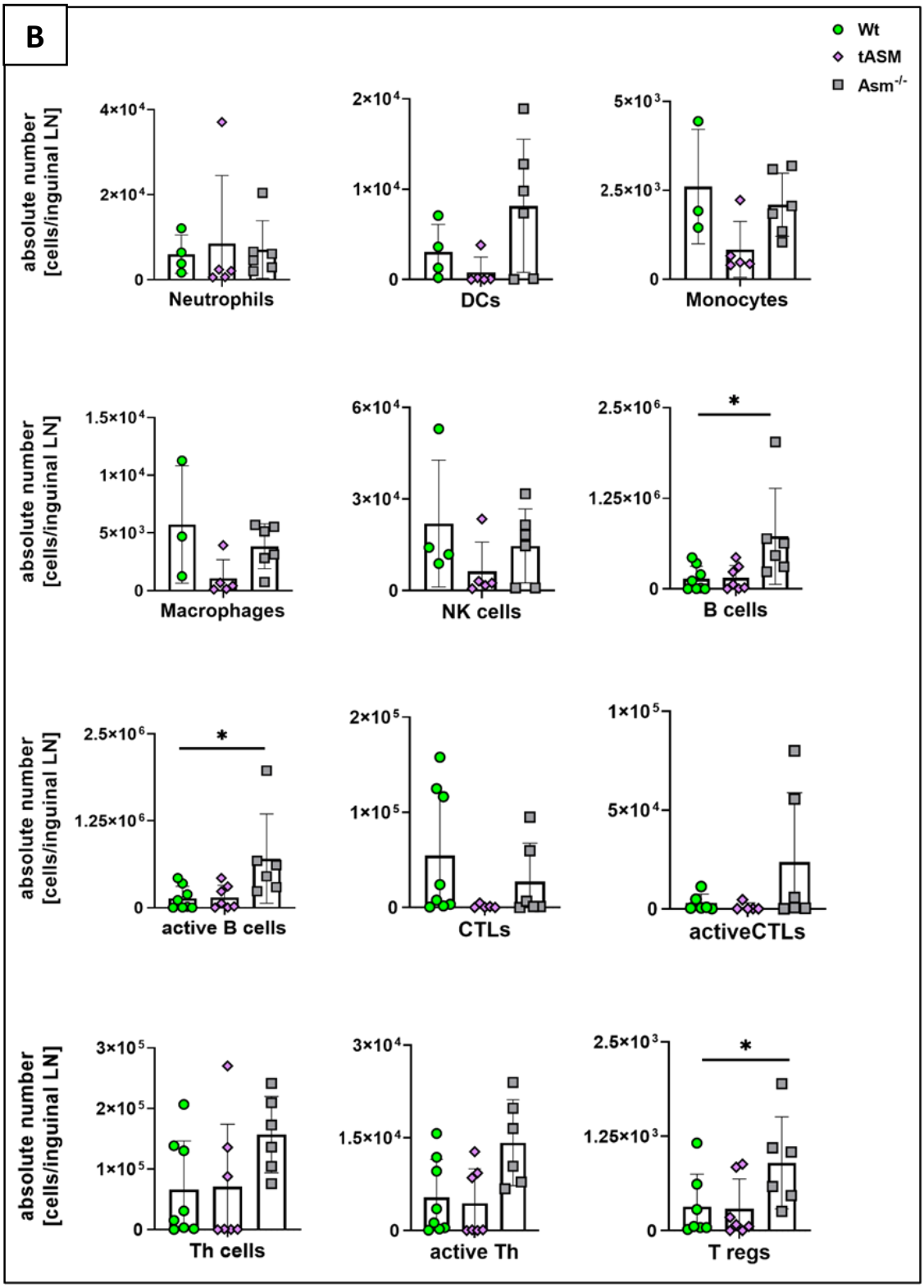
B
Wt
tASM
Asm-/-
absolute number [cells/inguinal LN]
Neutrophils
DCs
Monocytes
Macrophages
NK cells
B cells
active B cells
CTLs
activeCTLs
Th cells
active Th
T regs
*

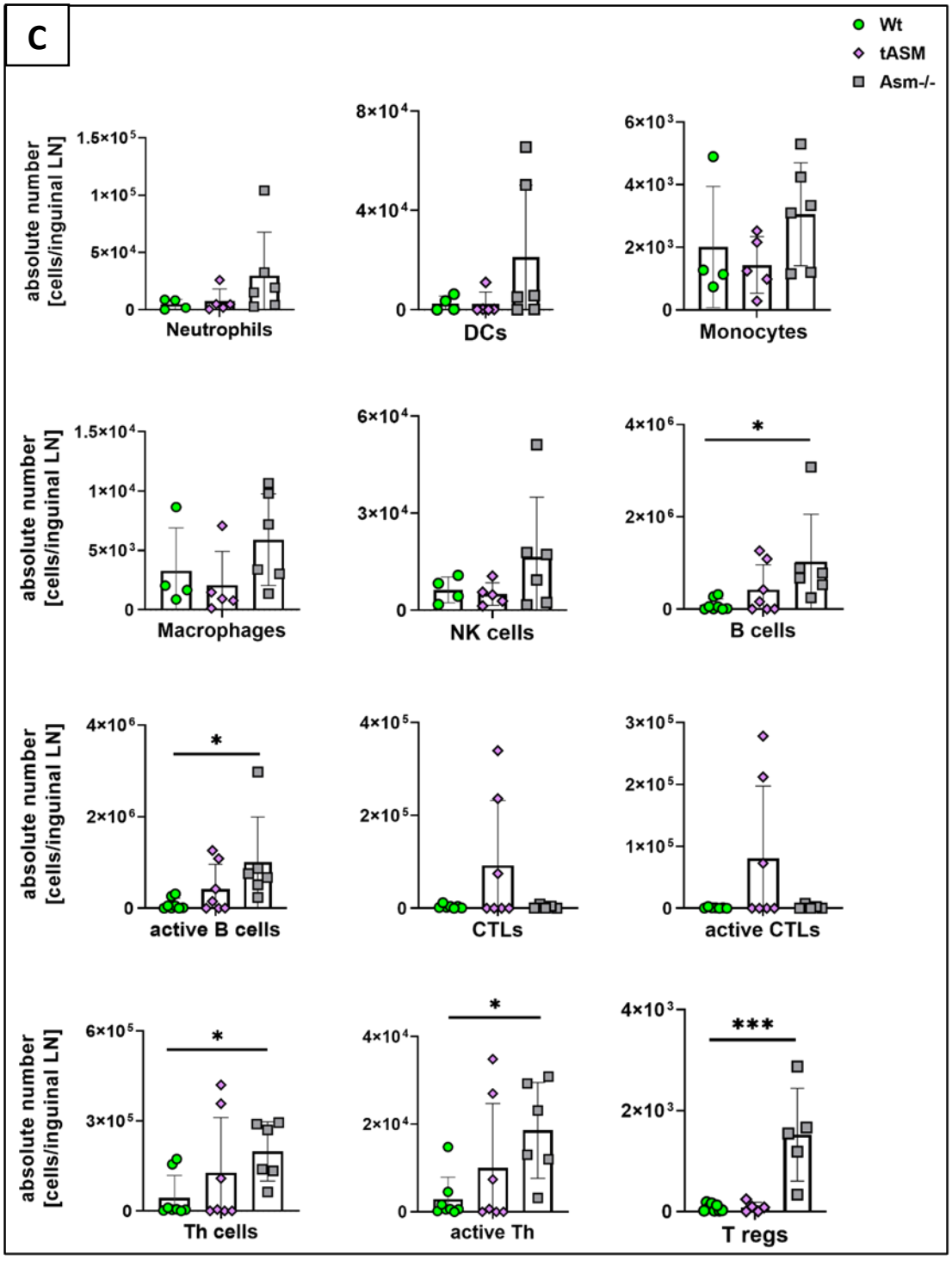

Figure 17. WBCs in inguinal lymph nodes 4 days after radiation

A) WBCs in control inguinal LN, B) in right inguinal LN and C) in left inguinal LN.

Mice were sacrificed 4 days after radiation, and both right and left inguinal were harvested to analyse their immune cells in the flow cytometry. Single-cell suspensions were obtained and cells were incubated with respective conjugated antibodies. Statistical significance between the three genotypes was determined by analysis of variance (one-

way ANOVA) followed by Bonferroni's selected comparisons test. P-values ($p \leq 0.05$, $p \leq 0.001$) are indicated by an asterisk * or ***, respectively. Outliers were excluded according to GraphPad statistical analyse. n: wt =6, tAsm= 6, $Asm^{-/-}$ =5.

3.7 Circulating WBCs after radiation

Since there is a connection between the abscopal effect and circulating WBCs, the migration of APCs and T-cells between tumor microenvironments, spleen, and inguinal LNs was observed after 4 days of radiation. Blood samples were taken from the tail veins and examined at VetABC blood counter. Although there is an abscopal effect in tAsm mice, no difference in their circulating WBCs was found compared to wt mice either with or without radiation (Figure. 18).

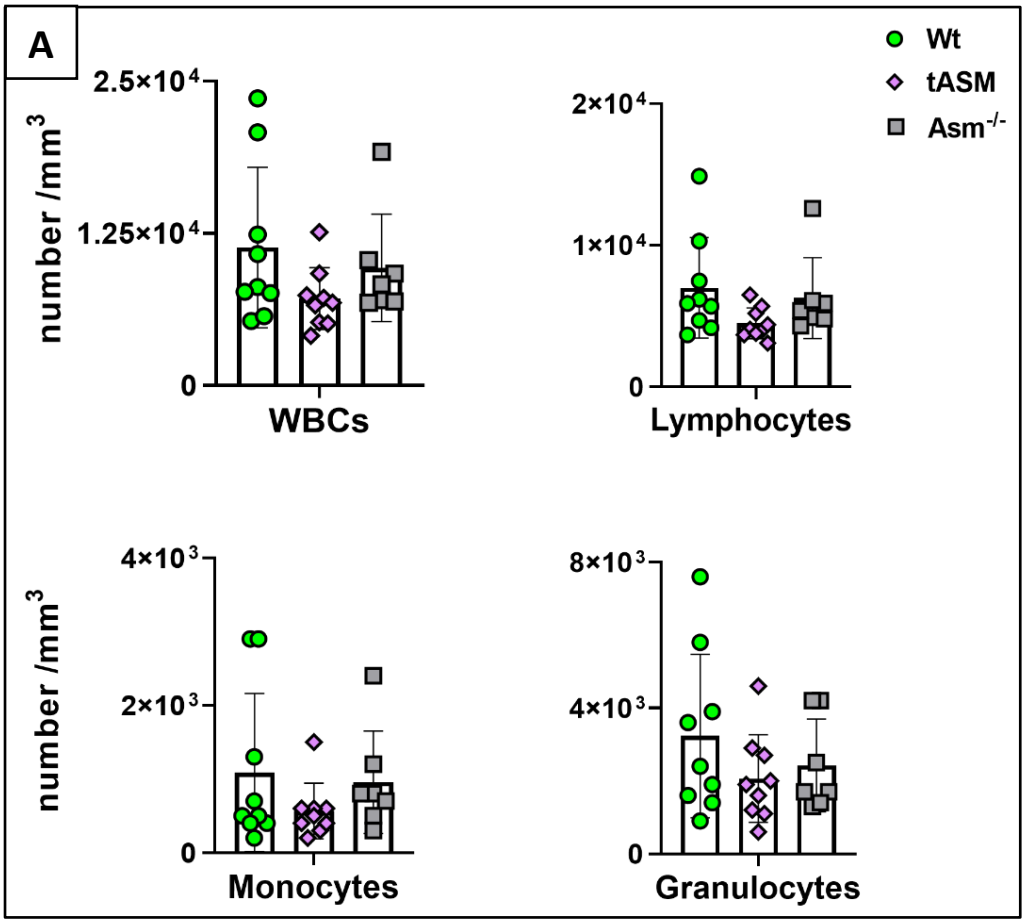

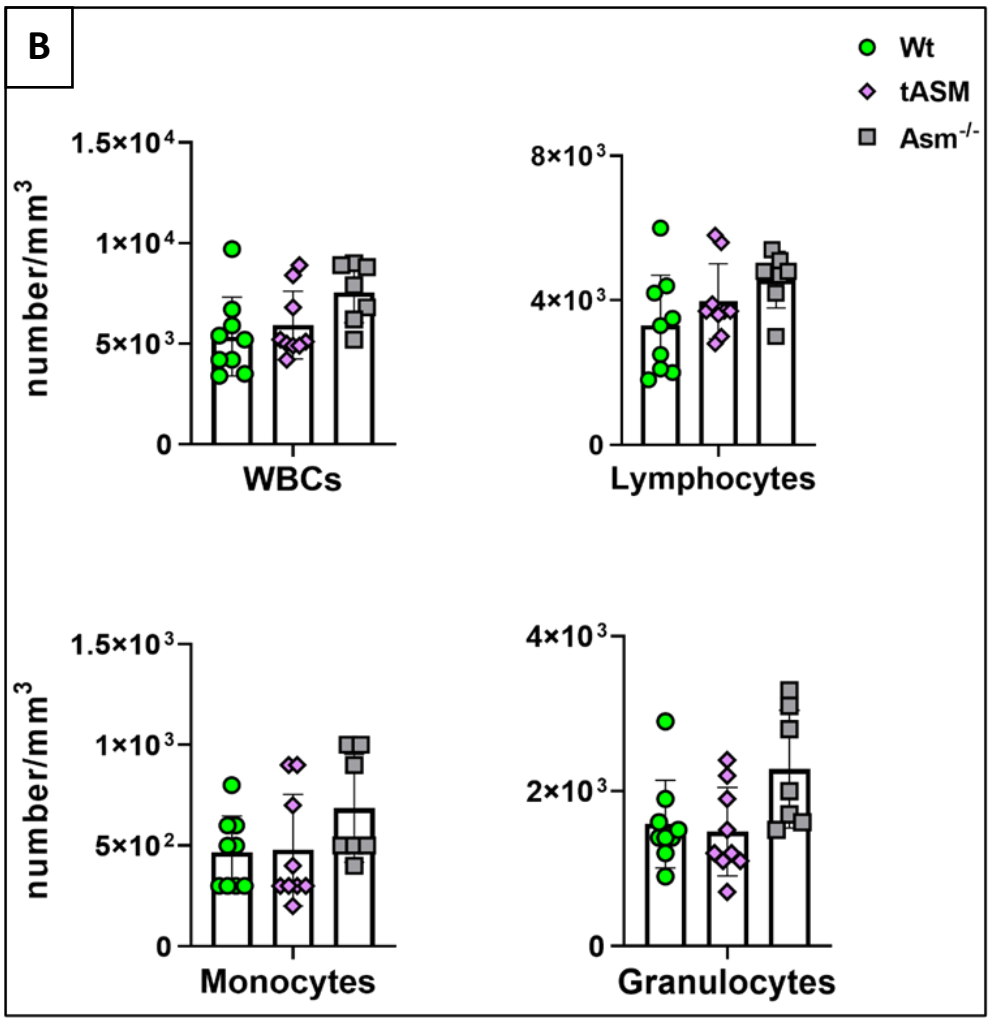

Figure 18. Circulating WBCs with or without radiation

A)- Circulating WBCs in control mice, B)- Circulating WBCs in radiated mice. Blood samples were collected 17 days post-implantation and gathered in K3EDTA tubes. The analysis was performed in SCIL abc vet, and the statistical significance between the three genotypes was determined by analysis of variance (one-way ANOVA) followed by Bonferroni's selected comparisons test. n: wt =9, tAsm= 9, $Asm^{-/-}$ =7.

3.8 No difference in the concentration of the cytokines whether Asm is expressed or not

Cytokines are the main factors in WBC's attraction to the site of inflammation or invasion. Therefore, studying their levels in the serum was commenced to investigate their relationship with the abscopal effect and Asm expression. Initially, a wide range of the serum cytokines was measured through the mouse cytokine panel array A. One mouse from each genotype, wt, tAsm and $Asm^{-/-}$, was elected 4 days after radiation. We speculated high levels of INF-γ, TNF, or IL-10 in tAsm mice; however, the assay revealed a virtual difference only in TIMP-1 and MCP-1 in $Asm^{-/-}$ mice compared to wt mice (Figure. 19). Therefore, further assessment through ELISA kits was followed. The serum was taken and diluted to proper concentration (1:6 for MCP1 and 1:15 for TIMP-1) and processed as explained in methods. In contrast to our findings in cytokine panel array A, no difference was observed in TIMP-1 and MCP-1 concentrations between the studied genotypes (Figure. 20).

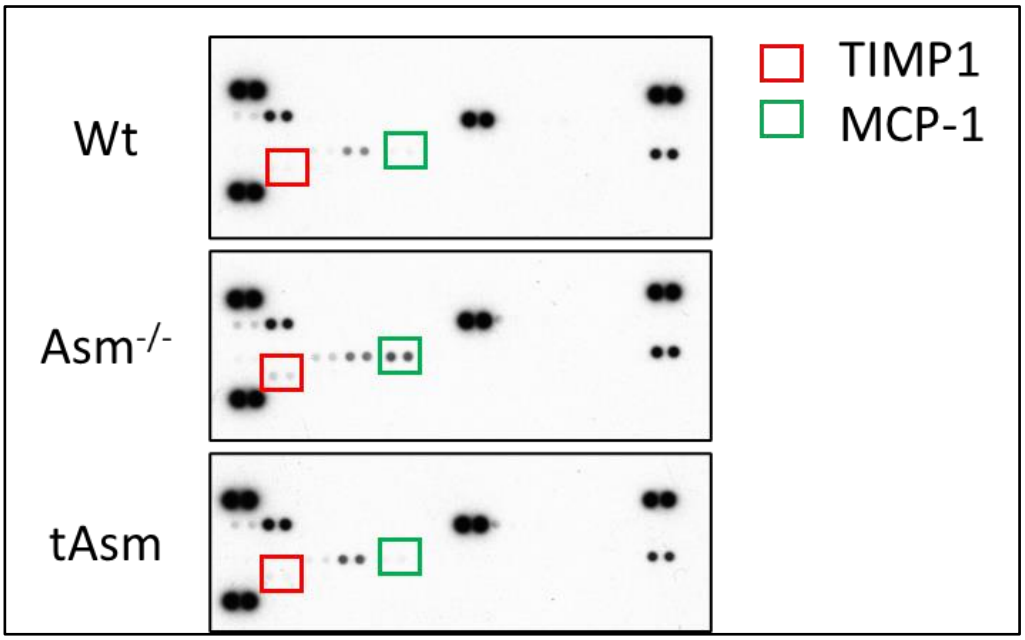

Figure. 19. Cytokines panel assay in serum

Blood samples were collected 4 days post-radiation, left to be clotted for 30 minutes and centrifuged 2000×g/ 20 min/RT, and serum was collected. 70 µl of serum was taken and processed in cytokine panel array A kit according to the provided protocol. n: wt=1, tAsm=1, $Asm^{-/-}$ =1.

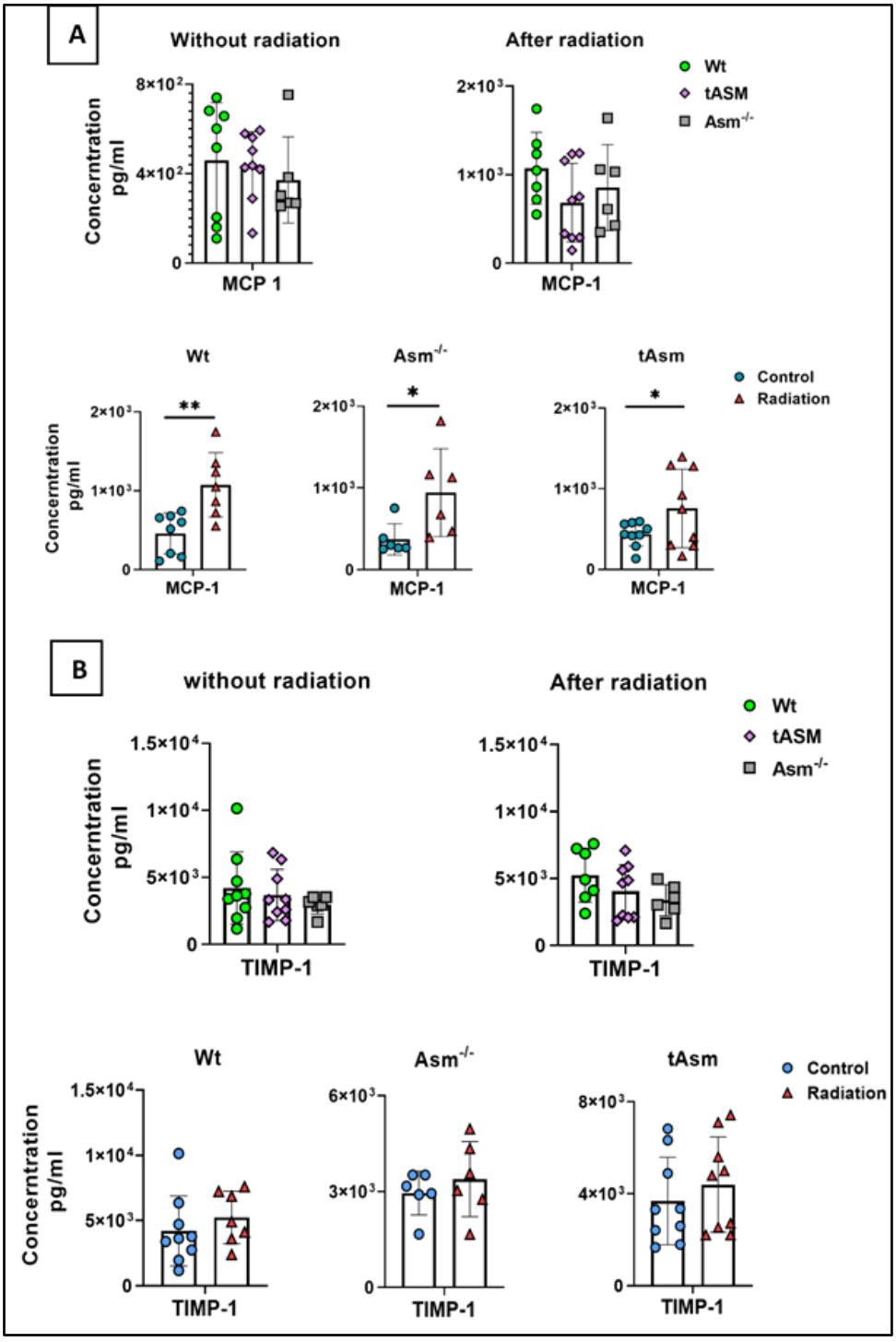

Figure. 20. MCP-1 and TIMP-1 concentration in serum

A)- MCP-1 concentration and B)- TIMP-1 concentration in serum. Blood samples were obtained 17 days post-implantation or 4 days post-radiation. Protein concentration was detected for each sample, and data were quantified to observe the statistical difference by one-way ANOVA and student t-test. Given are the mean ± SD from 3 independent studies. n: wt=9, tAsm=9, $Asm^{-/-}$=6.

4. Discussion

4.1 Radiation controlled tumor growth regardless of Asm expression

Sphingolipids have bioactive effects on cancer itself and its microenvironment, and targeting the main two central molecules of sphingolipids metabolism, ceramide and S1P, could be an approach to follow along with radiation in treating cancer (Furuya et al., 2011). In this study, we investigated whether Asm has a direct influence on immune response against tumor growth side by side to ceramide-induced apoptosis. TME provides the tumor its requirements to persist, and it involves various cytokines that promote neovascularization and formation of TAMs, MDSCs and Tregs, which also enhance tumor vascularization and suppresses the infiltrated APCs and T-cells. Therefore, the additional investigated factor was the immune response after tumor radiation and its association with Asm. Initially, the impact of Asm on tumor evolution was identified via following LLC growth with and without radiation in three Asm expression states, wt, tAsm and $Asm^{-/-}$. The tumors in $Asm^{-/-}$ mice showed more rapid growth comparing with the other genotypes when not irradiated (Figure. 10). One hypothesis to explain this finding is the differential prosper of new vessels in the TME, which is induced by angiogenic factors like vascular endothelial growth factor (VEGF), platelet-derived growth factor (PDGF), transforming growth factor β (TGF-β), hepatocyte growth factor (HGF), and basic fibroblast growth factor (bFGF) which was described by (Tonini et al., 2003). TAMs typically behave as M2 macrophages, playing a pivotal role in the TME. The interaction between the tumor cells and TAMs is promoted via macrophage colony-stimulating factor, and they produce various growth factors such as bFGF, HGF, PDGF, VEGF and matrix metalloproteinase 9 (MMP-9) (Lamagna et al., 2006). Moreover, Tregs play an active role in the progression of tumors via secreting TGF-β and IL-10, which support neovascularization and suppress the T-cells and APCs (Vignali et al., 2008). Therefore, the concomitant presence of TAMs and Tregs with a possible low formation of ceramide in tumors of $Asm^{-/-}$ mice could explain the rapid tumor growth in this genotype induced by the secretions of these cells. When tumors were radiated, all primary tumors in all genotypes showed a decrease in their growth rate, including tumors in

$Asm^{-/-}$ mice, representing a response to radiation (Figure. 10). This outcome is at the first view in contrast to the findings from Garcia-Barros et al. The resistance in $Asm^{-/-}$ mice to tumor radiation, which was witnessed in her experiments (Garcia-Barros et al., 2003), was explained with reduced apoptosis in the endothelial cells due to the absence of ceramide. One difference to our experiments is that Garcia-Barros injected in her experiment's melanoma and fibrosarcoma cells, whereas Lewis lung carcinoma were injected subcutaneously in our study. Therefore, a heterotropic tumor model was applied in our research, whereas Garcia-Barros applied an orthotopic tumor model. Orthotopic tumor models have different TME features than heterotopic tumor models, which may make them more radioresistant. It was mentioned by Erstad et al.; that heterotropic tumors have a slower growth rate comparing to orthotopic tumors, and this was correlated with a significant decrease in the cell proliferation manifested by a reduction in Ki67 expression (Erstad et al., 2018). Furthermore, a study was performed by Lee et al. to investigate the difference in TME between heterotopic and orthotopic hepatic tumors after radiation displayed more vascularization and micro vessel density in orthotopic tumors, which was approved via high expression of VEGF and CD31, respectively. Moreover, COX-2, a key regulator in the TME that inhibits apoptosis and stimulates angiogenesis, and MDSCs, were higher in orthotopic tumors, and all these aspects in orthotopic tumors make them more resistant to radiation than the heterotropic tumors (Lee et al., 2016). Therefore, this obvious difference in vascularization between orthotopic and heterotopic tumors may be responsible our divergent finding.

4.2 Asm regulates the tumor microenvironment immunity and its overexpression arouses the abscopal effect

An abscopal effect is a desirable phenomenon in treating cancer since it helps to constrain the tumor's metastasis with minimum side effects upon local radiation. It was already approved that the abscopal effect is a consequence of the immune response against the radiated tumor (Demaria et al., 2004). The abscopal effect is triggered by presenting the released tumor antigens by the APCs to CTLs in the secondary lymphoid organs, lymph nodes and spleen, which stimulate their proliferation and activation to attack the radiated tumor and circulate to eliminate similar antigens far from the primary site (Grass et al., 2016). In this study, it was shown that radiating tumors in the right lower limb (primary

tumors) and preserving the tumors in the left side (secondary tumors) lead to a significant tumor growth regression of both primary and secondary tumors in tAsm mice and a tendency in tumor growth regression of secondary tumors in wt mice (Figure. 11). Therefore, it was warranted to observe the response of the immune cells in tumors to illustrate the abscopal effect in tAsm mice and its absence in $Asm^{-/-}$ mice. The tumor microenvironment is created by the tumor, and once it is established, it forms an effective barrier to immune cell functions. The immune effector cells, which are recruited to the tumor site, will be downregulated by various inhibitory cytokines disseminated in the TME and not only fail to attack the tumor, but they also will be co-opted to promote tumor growth. The main pro-tumorigenic immune cells which spread out in TME are MDSC, Tregs and TAMs. MDSCs are one of the significant components of the tumor microenvironment and they impose their immunosuppressive nature through deactivating DCs and CTLs, and the recruiting Tregs. In this study, control tumors were significantly infiltrated with PMN-MDSC at the earlier time point (4 days after radiation) (Figure. 13.A) and a subsequent drop in neutrophils, DCs and monocytes numbers was detected at the latest time point (10 days after radiation) in $Asm^{-/-}$ mice (Figure. 12.A). Furthermore, radiating the tumors did not amend the inhibitory nature in $Asm^{-/-}$ mice because of the accumulation of TAMs and Tregs in their primary tumors at the early point (Figure. 13.B). Similar findings were reported by Assi et al. (Assi et al., 2015) who conducted her experiments by injecting melanoma cells in which Asm was either downregulated or maintained at high levels. She found a significant increase in MDSCs and Tregs infiltration in $Asm^{-/-}$ mice, which was accompanied by accumulation of interleukin IL-10, GM-CSF, and TGF-β1 and lower DCs recruitment which displayed an immature and anergic phenotype as indicated by the reduction of the costimulatory markers CD80 and MHCII. However, the high expression of Asm in melanoma cells encountered all these outcomes. This was illustrated in our study, when the implanted tumors in tAsm mice recruited more DCs and intermediate monocytes with developing less Tregs and MDSCs at the early time point either without radiation (Figure. 13.A) or after radiation (Figure. 13.B). An explanation to decreased formation of MDSCs in Asm overexpression status was offered by Liu et al. (Liu et al., 2016). He detected a significant decrease in MDSCs accumulation in vivo after treating tumor-bearing mice with LCL521, an inhibitor of lysosomal acid ceramidase. He indicated that the lysosome is a major target

of LCL521 action and potentially increase C16 ceramide levels, which initiate the apoptosis pathway along with activating cathepsin B and cathepsin D to heighten MDSCs death. Based on these findings, ceramide accumulation and apoptosis in MDSCs due to Asm overexpression was speculated in our study. NK cells provide the first line of defence against tumor cells and function without the requirement for prolonged pre-activation as CTLs. Detecting the recruitment of NK cells in our study revealed higher numbers in the late endpoint in both primary (Figure. 12.B) and secondary (Figure. 12.C) tumors of $Asm^{-/-}$ mice. However, this increase in NK cells was absent in the early endpoint. The survival of NK cells in the tumor microenvironment could be explained by less accumulation of the intracellular ceramide. Taguchi et al. explored the effect of IL-2 on NK cells survival. He found that KHYG-1 cells' growth was increased when they were cultured with IL-2, and the deprivation of IL-2 decreased the KHYG-1 growth rate. The IL-2 with Inositol phosphatidyl 3 (IP3) involvement decreases ceramide formation in NK cells through inhibition of Asm and activation of Glucosylceramide synthase (GCS) and sphingomyelin synthase (SMS) (Taguchi et al., 2004). In our experiment, Asm was already absent in $Asm^{-/-}$ mice, which reduced the accumulation of ceramide in the NK cell and prolonged their survival in the TME. Still, the diffusion of MDSCs, Tregs and TAMs in the primary and secondary tumors of this genotype probably disrupted the infiltrated NK cells and supported their continuous growth. Regarding the infiltration in the secondary tumors, our data revealed a significant induction of TAMs and Tregs in the early endpoint (Figure. 13.C) and late endpoint (Figure. 12.C) in $Asm^{-/-}$ mice; otherwise, significant recruitment of DCs and intermediate monocytes was witnessed in the early endpoint in tAsm mice (Figure. 13.C). Taken together, these data support the assumption that Asm plays a role in the tumor immune-toxicity through enhancing the immune effector cells and conquering the immune inhibitor cells in the tumor microenvironment. Controversially, some studies reported that Asm either has no role in the immune response against the tumor or has a pro-tumorigenic effect. An investigation revealed that the regression in tumor development is achieved by the endothelial cell’s apoptosis after radiation, and observing the immune cells in the radiated tumors revealed a comparable infiltration of T-cells, B cells and NK cells in the implanting MCA/129 fibrosarcoma and B16F1 melanomas in $Asm^{-/-}$ mice and wt mice (Garcia-Barros et al., 2004). This comparable infiltration was also seen in our experiments. However, we proved that

numbers of Tregs and TAMs were higher when Asm is deficient, and the overexpression of Asm decreased their formation in the TME and prompted DCs and monocytes migration to the tumor sites, which produced the abscopal effect. The other debatable point is that Asm promotes tumor progression. This was mentioned in a study on non-small lung cell carcinoma (NSCLC), which concluded that high Asm activity was found in the patients' serum (Kachler et al., 2017). The further investigation disclosed that deleting Smpd1 in lung carcinoma cell lines resulted in a decrease in tumor cell death and its proliferation, which was investigated through a Ki67 and PI staining and showed a cell-cycle arrest. Moreover, the reduction in tumor growth in $Asm^{-/-}$ mice was warranted by the antitumoral T-cell–mediated immune response. The infiltration of $CD4^{+}$ T-cells in lung cancer was observed in both wt and $Asm^{-/-}$ mice, and although no difference in the total number of $CD4^{+}$ T-cells, a significant difference was detected in its subtypes. Unlike our findings, Tregs and Th 17 infiltration was similar in $Asm^{-/-}$ and wt mice; however, Th 1 the, important subtype in fighting the tumor, and its excreted IFN-γ levels were higher in $Asm^{-/-}$ mice. Besides, infiltrated CTLs have a comparable total number in $Asm^{-/-}$; still, more non-apoptotic CTLs were found in the lungs of tumor-bearing $Asm^{-/-}$ mice and upregulation of long memory markers such as CD117 and CD 127 along with T bet, the central transcription factor for the expression of IFN-γ, were also significant in $Asm^{-/-}$ mice. The distinction is Asm in the mentioned study was knocked out from the tumor cell line; however, Asm in our study was knocked out from the host; accordingly, the reaction of the host against the tumor was investigated in the different status of Asm plus the effect of radiation.

4.3 Asm in WBCs migration

In this study, it was presented that Asm affects Treg development in the spleen. Similar to tumors, Tregs were abundant in $Asm^{-/-}$ mice with and without radiation either at the early endpoint (Figure. 15) or at the late endpoint (Figure. 14). These findings in line with conclusions announced by Zhou et al. which revealed that lacking Asm generated ceramide leads to increased induction of iTreg in spleens of $Asm^{-/-}$ mice. This effect was probably due to the circulated cytokines TGF-β and IL-10. Besides, $Asm^{-/-}$ mice that have enhanced iTreg are also able to lose the Foxp3 induction when treated with ceramide (Zhou et al., 2016). Neutrophils recirculate between the secondary lymph organs and

different tissues and play a role in the innate immune response against extraneous cells. Therefore, their recruitment in the spleen was investigated to assay their role in the abscopal effect. Sequestration of neutrophils was noticed in the spleens of $Asm^{-/-}$ mice after radiation either at the early endpoint (Figure. 15) or at the late endpoint (Figure. 14). The reason behind this result was not investigated in this study; however, Bogoslowski et al. found that neutrophils recirculate between the lymph nodes as they enter the lymph node via L-selectin and egress via an S1P dependent mechanism, and this was confirmed by the accumulation of neutrophils in the lymph nodes after treating with FTY720 (Bogoslowski et al., 2020). Since S1P is the second metabolite of Asm, a limited generation of it in $Asm^{-/-}$ mice could explain the elevation of neutrophils in their spleens. The investigated inguinal lymph nodes in tAsm mice were characterized by high CTLs proliferation and NK cell recruitment but declined Tregs formation after 10 days of radiation (Figure. 16.B). Otherwise, the recruitment of monocytes, macrophages and dendritic cells was significantly decreased, plus Tregs numbers were higher in $Asm^{-/-}$ after radiation either at the late endpoint (Figure. 16.B) or at the earlier time point (Figure. 17.B.C). Moreover, CTLs were less in control inguinal lymph nodes of $Asm^{-/-}$ mice (Figure. 14, Figure. 16). The impact of Asm on T-cells development was studied by Hose. et al., and he witnessed a less formation of Tregs in Asm overexpressed T-cells, which was also detected in this study, and advanced differentiation to Th1 cells; moreover, the Asm overexpressing T-cells displayed elevated TCR expression and increased proliferation and activation, which resulted in diminishing the parasitemia comparing to control group (Hose et al., 2019), and this could also be a reason for the CTLs effectiveness against primary and secondary tumors in tAsm mice. Furthermore, when DCs sense the tumor-associated molecular patterns after radiation, they undergo maturation, which involves the upregulation of molecules for Ag presentation and the T lymphocytes stimulation. Pritzl et al. provided evidence that exogenous administration of ceramide analogue induces maturation of DCs and robust CTLs and Th response against LCMV infection. He found that incubating the DCs with C8 ceramide elevated the expression of MHC-I, MHC-II, CD80 and CD86 on DCs upon LCMV infection, and this induced a higher proliferation of CTLs comparing to non-treated cells (Pritzl et al., 2015). Hence, the upgraded maturation of DCs prompted by the accumulated ceramide could be the reason behind the robust proliferation and activation of T-cells in the inguinal lymph

nodes of tAsm mice and the abscopal effect; besides the decrease in DCs recruitment in $Asm^{-/-}$ mice.

4.4 Asm correlation with MCP-1 and TIMP-1

Cytokines produced by the tumor microenvironment and the infiltrated immune cells play an essential role in tumor regression or progression. Although we expected to find different cytokine serum levels, regarding the different mouse phenotypes, when comparing a panel of 40 different cytokines, we found only two which were secreted in different amounts. MCP-1 and TIMP-1 seemed to be higher in $Asm^{-/-}$ mice comparing to the other two genotypes (Figure. 19). The panel assay was conducted through cytokine panel array A, which is a western blot test, using one irradiated mouse of each genotype. To have a more accurate result, a further investigation was performed with the more sensitive test ELISA in several mice. The main activity of the Monocyte chemoattractant protein-1 (MCP-1) is to recruit blood monocytes into sites of inflammation and tumors and after evaluating the data from the cytokine array by ELISA, no difference was witnessed between Asm-/- mice and other genotypes (Figure. 20.A). Still, a difference between the control group and the radiated group was noticed in each genotype, which could verify the infiltration of macrophages in tumors only after radiation (Figure. 20.A). The tissue inhibitor of metalloproteinases 1 (TIMP-1) is an endogenous inhibitor for matrix metalloproteinases (MMPs) responsible for remodelling the extracellular matrix and is involved in migration, invasion and metastasis of tumor cells. Similar to MCP-1, TIMP-1 levels were unrelated to Asm expression, and no difference was witnessed in ELISA assay between the studied genotypes (Figure. 20.B).

5. Conclusion and outlook

In this work, we presented a descriptional study of the immune cells in tumors, spleens and inguinal lymph nodes either with or without radiation in different Asm expression statuses (Table. 2, 3, 4). However, the mechanism of the recruitment and migration of the immune cells towards the tumors and the role of Asm within was not investigated. Moreover, the cytotoxicity of the CTLs against the tumors, whether through excretion of the cytotoxic granules or PD-L integration and the inhibitory functions of the TAMs or Tregs in the tumor microenvironment and its association to Asm levels requires further inspection. Besides, cytokines in serum were measured; however, the tumor microenvironment cytokines were skipped because of the sample shortage. Another speculation about the restricted growth in the secondary tumors of tAsm mice after the local radiation is the apoptosis induction via the Asm in serum released from either the RBCs (Bode et al., 2010) or the platelets (Dahm et al., 2006), which initiate the degradation of sphingomyelin and ceramide accumulation in tumor cells. Consequently, a further assay of Asm level in the serum of the different genotypes and histochemistry sections with TUNEL staining of the secondary tumors should be considered.

Tumor												
After 10 days						After 4 days						
Control		primary		secondary		Control		primary		secondary		
$Asm^{-/-}$	tAsm	$Asm^{-/-}$	tAsm	$Asm^{-/-}$	tAsm	$Asm^{-/-}$	tAsm	$Asm^{-/-}$	tAsm	$Asm^{-/-}$	tAsm
↓ mono	-	↑ Mac	↓ DCs	↑ mac	-	↑ PMN-MDCSS	↑ DCs	↑ TAMs	↑ DCs	↑ TAMs	↑ DCs
↓ DCs	-	↑ NK cells		↑ NK cells	-		↑ Im		↑ Im	↑ Th	↑ Im
		↑ Tregs								↑ Tregs	

Mono: monocytes, DCs: dendritic cells, Mac: macrophages, PMN-MDCS: polymorphonuclear myeloid derived suppressor cells, Im: intermediate monocytes, TAMs: tumor associated macrophage, Tregs: regulator T cells, NK cells: natural killer cells

Table 2. Summarize The infiltrated immune cells in tumor and its ‘differences comparing to wt genotype

Spleen												
After 10 days						After 4 days						
Control		radiated				Control				radiated		
$Asm^{-/-}$	tAsm	$Asm^{-/-}$	tAsm			$Asm^{-/-}$	tAsm			$Asm^{-/-}$	tAsm	
↑ Mac	-	↑ Mac	↑ mono			↓ NK cells	↑ mono			↑ Neutrophils	-	
↑ Tregs	-	↑ Neutrophils				↓ B cells	↑ B cells			↑ DCs	-	
						↓ Active B cells	↑ Active B cells			↑ Tregs	-	

Mono: monocytes, DCs: dendritic cells, Mac: macrophages, Tregs: regulator T cells, NK cells: natural killer cells

Table 3. Summarize the WBCs in spleen and its ‘differences comparing to wt genotype

Inguinal lymph nodes											
After 10 days				After 4 days							
Control		radiated		control		right LNs		left LNs			
$Asm^{-/-}$	tAsm	$Asm^{-/-}$	tAsm	$Asm^{-/-}$	tAsm	$Asm^{-/-}$	tAsm	$Asm^{-/-}$	tAsm		
CTLs	Mac	neutrophils	CTLs	mono	-	B cells	-	B cells	-		
Active CTLs		B cells	NK cells	CTLs	-	Active B cells	-	Active B cells	-		
Th		DCs	Tregs	Active CTLs	-			Tregs	-		
Active Th		mono		Th	-						
				Active Th	-						
				B cells	-						
				Active B cells							

Mono: monocytes, DCs: dendritic cells, Mac: macrophages, Tregs: regulator T cells, NK cells: natural killer cells, CTLs: cytotoxic T lymphocytes, Th: T helper cells

Table 4. Summarize the WBCs in inguinal lymph nodes and its ‘differences comparing to wt genotype

6. Summary

Several studies revealed that radiation stimulates tumor-specific immunity in the radiated area as well as in distant areas supposedly responsible for abscopal effects. In radiation-induced cellular stress, acid sphingomyelinase (Asm) catalyzes the hydrolysis of sphingomyelin to ceramide. Garcia Barros and colleagues have found that tumor growth was delayed in wild type (wt) mice upon radiation, whereas the sensitivity of the tumor to radiation was much less in acid sphingomyelinase deficient ($Asm^{-/-}$) mice. This was attributed to reduced endothelial microvascular apoptosis in $Asm^{-/-}$ mice due to inefficient formation of ceramide. However, the role of the immune response was not investigated, which raises the questions whether the immune system participates in tumor regression after radiation, and whether there is a connection between Asm, ceramide and immune response. Therefore, a dual-tumor was injected subcutaneously in both lower limbs. The tumors in the right limb were solely radiated with a single dose of 15 Gy (the primary tumor) whereas the versus tumors (the secondary tumor) were spared from radiation. The reduction in growth rate in the secondary tumors due to immune cells infiltration is considered as abscopal effect. To address the role of the Asm/ceramide system in the response of the immune system to irradiation. Our trials were conducted in three different genotypes, i.e. wild type (wt) mice, mice overexpressing the acid sphingomyelinase (tAsm), and mice lacking the acid sphingomyelinase ($Asm^{-/-}$). We found a regression in primary tumors in all genotypes after a single dose of 15 Gy. Furthermore, a regression in secondary tumors was found in tAsm mice, but not in wt and $Asm^{-/-}$ mice. Measurement of immune cell infiltration let us suggest that the abscopal effect is attributable to the immune system. In tAsm mice, we found higher antigen presenting cells (APCs) in tumors and higher APCs and effector T-cells in inguinal lymph nodes possibly the reason for the abscopal effect. Further, we found an increase in Tregs and TAMs in $Asm^{-/-}$ mice which might be responsible for the abolished abscopal effect and faster growth rate. These data clearly show that acid sphingomyelinase is involved in the antitumor effect, most probably due to the effects on the immune response.

7. Zusammenfassung

Mehrere Studien zeigten, dass Bestrahlung die tumorspezifische Immunität stimulieren kann, welche sowohl im bestrahlten Bereich als auch in entfernten (abskopalen) Bereichen Wirkung entfaltet. Bei strahleninduziertem zellulärem Stress katalysiert die saure Sphingomyelinase (Asm) die Hydrolyse von Sphingomyelin zu Ceramid. Garcia Barros und Kollegen haben festgestellt, dass Bestrahlung zwar das Tumorwachstum bei Wildtyp-Mäusen (Wt) verzögerte, auf Tumoren in saure Sphingomyelinase-defizienten ($Asm^{-/-}$) Mäusen hingegegn praktisch keine Wirkung hatte. Dies wurde auf eine verringerte endotheliale mikrovaskuläre Apoptose bei $Asm^{-/-}$ Mäusen aufgrund einer ineffizienten Bildung von Ceramid zurückgeführt. Daten über die Rolle der Immunantwort sind diesbezüglich jedoch nicht veröffentlicht. Im vorliegendem Projekt soll untersucht werden, ob das Immunsystem nach Bestrahlung an der Tumorregression beteiligt ist und ob ein Zusammenhang zwischen Asm und Immunantwort besteht. Um dies zu beantworten, wurde ein Doppeltumor-Modell verwendet, bei dem nur ein Tumor (der Primärtumor) bestrahlt wurde, um die lokale (im Primärtumor) und die systemische Immunantwort der Behandlung außerhalb des Strahlenfeldes (im Sekundärtumor) zu analysieren. Die Versuche wurden an drei verschiedenen Genotypen durchgeführt, wt, saure Sphingomyelinase überexprimierende tAsm und $Asm^{-/-}$ Mäusen. Wir fanden eine Regression der Primärtumoren in allen Genotypen nach einer Einzeldosis von 15 Gy. Darüber hinaus wurde bei tAsm Mäusen eine Regression der sekundären Tumore im Sinne eines abskopalen Effekts nachgewiesen, nicht jedoch bei wt und $Asm^{-/-}$ Mäusen. Unsere Daten legen nahe, dass der abskopale Effekt möglicherweise auf das Immunsystem zurückzuführen ist. Bei tAsm Mäusen könnten höhere antigen presenting cells (APCs) in den Tumoren und höhere APCs und Effektor-T-Zellen in ihren Leistenlymphknoten der Grund für den abskopalen Effekt sein. Andererseits könnte der Anstieg von Tregs und tumorassoziierte Makrophagen bei $Asm^{-/-}$ Mäusen das Fehlen eines abskopalen Effektes und die schnellere Wachstumsrate erklären. Diese Daten zeigen, dass die saure Sphingomyelinase an der anti-Tumorreaktion beteiligt ist, höchstwahrscheinlich aufgrund einer Regulation der Immunantwort.

8. References:

1. <Ceramide induced cell death is independent of the Fas.pdf>.
2. ASSI, E., CERVIA, D., BIZZOZERO, L., CAPOBIANCO, A., PAMBIANCO, S., MORISI, F., DE PALMA, C., MOSCHENI, C., PELLEGRINO, P., CLEMENTI, E. & PERROTTA, C. 2015. Modulation of Acid Sphingomyelinase in Melanoma Reprogrammes the Tumour Immune Microenvironment. *Mediators Inflamm,* 2015**,** 370482.
3. BODE, C., SENSKEN, S. C., PEEST, U., BEUTEL, G., THOL, F., LEVKAU, B., LI, Z. G., BITTMAN, R., HUANG, T., TOLLE, M., VAN DER GIET, M. & GRALER, M. H. 2010. Erythrocytes Serve as a Reservoir for Cellular and Extracellular Sphingosine 1-Phosphate. *Journal of Cellular Biochemistry,* 109**,** 1232-1243.
4. BOGOSLOWSKI, A., WIJEYESINGHE, S., LEE, W. Y., CHEN, C. S., ALANANI, S., JENNE, C., STEEBER, D. A., SCHEIERMANN, C., BUTCHER, E. C., MASOPUST, D. & KUBES, P. 2020. Neutrophils Recirculate through Lymph Nodes to Survey Tissues for Pathogens. *J Immunol,* 204**,** 2552-2561.
5. BOUCHER, L. M., WIEGMANN, K., FUTTERER, A., PFEFFER, K., MACHLEIDT, T., SCHUTZE, S., MAK, T. W. & KRONKE, M. 1995. CD28 signals through acidic sphingomyelinase. *J Exp Med,* 181**,** 2059-68.
6. BRAS, A., ALBAR, J. P., LEONARDO, E., DE BUITRAGO, G. G. & MARTINEZ, A. C. 2000. Ceramide-induced cell death is independent of the Fas/Fas ligand pathway and is prevented by Nur77 overexpression in A20 B cells. *Cell Death Differ,* 7**,** 262-71.
7. BROWN, D. A. & LONDON, E. 1998. Functions of lipid rafts in biological membranes. *Annu Rev Cell Dev Biol,* 14**,** 111-36.
8. CAMPHAUSEN, K., MOSES, M. A., MENARD, C., SPROULL, M., BEECKEN, W. D., FOLKMAN, J. & O'REILLY, M. S. 2003. Radiation abscopal antitumor effect is mediated through p53. *Cancer Res,* 63**,** 1990-3.
9. CARPINTEIRO, A., BECKER, K. A., JAPTOK, L., HESSLER, G., KEITSCH, S., POZGAJOVA, M., SCHMID, K. W., ADAMS, C., MULLER, S., KLEUSER, B., EDWARDS, M. J., GRASSME, H., HELFRICH, I. & GULBINS, E. 2015. Regulation of hematogenous tumor metastasis by acid sphingomyelinase. *EMBO Mol Med,* 7**,** 714-34.
10. DAHM, F., NOCITO, A., BIELAWSKA, A., LANG, K. S., GEORGIEV, P., ASMIS, L. M., BIELAWSKI, J., MADON, J., HANNUN, Y. A. & CLAVIEN, P. A. 2006. Distribution and dynamic changes of sphingolipids in blood in response to platelet activation. *J Thromb Haemost,* 4**,** 2704-9.
11. DEMARIA, S., NG, B., DEVITT, M. L., BABB, J. S., KAWASHIMA, N., LIEBES, L. & FORMENTI, S. C. 2004. Ionizing radiation inhibition of distant untreated tumors (abscopal effect) is immune mediated. *Int J Radiat Oncol Biol Phys,* 58**,** 862-70.
12. EDIMECHEVA, I. P., KISEL, M. A., SHADYRO, O. I., VLASOV, A. P. & YURKOVA, I. L. 1997. The damage to phospholipids caused by free radical attack on glycerol and sphingosine backbone. *Int J Radiat Biol,* 71**,** 555-60.
13. ERSTAD, D. J., SOJOODI, M., TAYLOR, M. S., GHOSHAL, S., RAZAVI, A. A., GRAHAM-O'REGAN, K. A., BARDEESY, N., FERRONE, C. R., LANUTI, M., CARAVAN, P., TANABE, K. K. & FUCHS, B. C. 2018. Orthotopic and heterotopic murine models of pancreatic cancer and their different responses to FOLFIRINOX chemotherapy. *Dis Model Mech,* 11.
14. FURUYA, H., SHIMIZU, Y. & KAWAMORI, T. 2011. Sphingolipids in cancer. *Cancer Metastasis Rev,* 30**,** 567-76.

15. GARCIA-BARROS, M., LACORAZZA, D., PETRIE, H., HAIMOVITZ-FRIEDMAN, A., CARDON-CARDO, C., NIMER, S., FUKS, Z. & KOLESNICK, R. 2004. Host acid sphingomyelinase regulates microvascular function not tumor immunity. *Cancer Res,* 64**,** 8285-91.
16. GARCIA-BARROS, M., PARIS, F., CORDON-CARDO, C., LYDEN, D., RAFII, S., HAIMOVITZ-FRIEDMAN, A., FUKS, Z. & KOLESNICK, R. 2003. Tumor response to radiotherapy regulated by endothelial cell apoptosis. *Science,* 300**,** 1155-9.
17. GRASS, G. D., KRISHNA, N. & KIM, S. 2016. The immune mechanisms of abscopal effect in radiation therapy. *Curr Probl Cancer,* 40**,** 10-24.
18. GRASSME, H., JEKLE, A., RIEHLE, A., SCHWARZ, H., BERGER, J., SANDHOFF, K., KOLESNICK, R. & GULBINS, E. 2001a. CD95 signaling via ceramide-rich membrane rafts. *J Biol Chem,* 276**,** 20589-96.
19. GRASSME, H., SCHWARZ, H. & GULBINS, E. 2001b. Molecular mechanisms of ceramide-mediated CD95 clustering. *Biochem Biophys Res Commun,* 284**,** 1016-30.
20. GULBINS, E. & KOLESNICK, R. 2002. Acid sphingomyelinase-derived ceramide signaling in apoptosis. *Subcell Biochem,* 36**,** 229-44.
21. HERZ, J., PARDO, J., KASHKAR, H., SCHRAMM, M., KUZMENKINA, E., BOS, E., WIEGMANN, K., WALLICH, R., PETERS, P. J., HERZIG, S., SCHMELZER, E., KRONKE, M., SIMON, M. M. & UTERMOHLEN, O. 2009. Acid sphingomyelinase is a key regulator of cytotoxic granule secretion by primary T lymphocytes. *Nat Immunol,* 10**,** 761-8.
22. HORINOUCHI, K., ERLICH, S., PERL, D. P., FERLINZ, K., BISGAIER, C. L., SANDHOFF, K., DESNICK, R. J., STEWART, C. L. & SCHUCHMAN, E. H. 1995. Acid sphingomyelinase deficient mice: a model of types A and B Niemann-Pick disease. *Nat Genet,* 10**,** 288-93.
23. HOSE, M., GUNTHER, A., ABBERGER, H., BEGUM, S., KORENCAK, M., BECKER, K. A., BUER, J., WESTENDORF, A. M. & HANSEN, W. 2019. T Cell-Specific Overexpression of Acid Sphingomyelinase Results in Elevated T Cell Activation and Reduced Parasitemia During Plasmodium yoelii Infection. *Front Immunol,* 10**,** 1225.
24. KACHLER, K., BAILER, M., HEIM, L., SCHUMACHER, F., REICHEL, M., HOLZINGER, C. D., TRUMP, S., MITTLER, S., MONTI, J., TRUFA, D. I., RIEKER, R. J., HARTMANN, A., SIRBU, H., KLEUSER, B., KORNHUBER, J. & FINOTTO, S. 2017. Enhanced Acid Sphingomyelinase Activity Drives Immune Evasion and Tumor Growth in Non-Small Cell Lung Carcinoma. *Cancer Res,* 77**,** 5963-5976.
25. KAM, W. W. & BANATI, R. B. 2013. Effects of ionizing radiation on mitochondria. *Free Radic Biol Med,* 65**,** 607-619.
26. KOLESNICK, R. N., GONI, F. M. & ALONSO, A. 2000. Compartmentalization of ceramide signaling: physical foundations and biological effects. *J Cell Physiol,* 184**,** 285-300.
27. LAMAGNA, C., AURRAND-LIONS, M. & IMHOF, B. A. 2006. Dual role of macrophages in tumor growth and angiogenesis. *J Leukoc Biol,* 80**,** 705-13.
28. LEE, I. J., LEE, E. J., PARK, H., KIM, W., HA, S. J., SHIN, Y. K. & SEONG, J. 2016. Altered Biological Potential and Radioresponse of Murine Tumors in Different Microenvironments. *Cancer Res Treat,* 48**,** 727-37.
29. LIU, F., LI, X., LU, C., BAI, A., BIELAWSKI, J., BIELAWSKA, A., MARSHALL, B., SCHOENLEIN, P. V., LEBEDYEVA, I. O. & LIU, K. 2016. Ceramide activates lysosomal cathepsin B and cathepsin D to attenuate autophagy and induces ER stress to suppress myeloid-derived suppressor cells. *Oncotarget,* 7**,** 83907-83925.
30. MARTIN, M., WEI, H. & LU, T. 2016. Targeting microenvironment in cancer therapeutics. *Oncotarget,* 7**,** 52575-52583.
31. OGRETMEN, B. 2006. Sphingolipids in cancer: regulation of pathogenesis and therapy. *FEBS Lett,* 580**,** 5467-76.
32. OGRETMEN, B. & HANNUN, Y. A. 2004. Biologically active sphingolipids in cancer pathogenesis and treatment. *Nat Rev Cancer,* 4**,** 604-16.

33. OKUMA, K., YAMASHITA, H., NIIBE, Y., HAYAKAWA, K. & NAKAGAWA, K. 2011. Abscopal effect of radiation on lung metastases of hepatocellular carcinoma: a case report. *J Med Case Rep,* 5**,** 111.
34. PENG, Q., QIU, X., ZHANG, Z., ZHANG, S., ZHANG, Y., LIANG, Y., GUO, J., PENG, H., CHEN, M., FU, Y. X. & TANG, H. 2020. PD-L1 on dendritic cells attenuates T cell activation and regulates response to immune checkpoint blockade. *Nat Commun,* 11**,** 4835.
35. PINHEIRO, M. A. L., KROON, J., HOOGENBOEZEM, M., GEERTS, D., VAN HET HOF, B., VAN DER POL, S. M. A., VAN BUUL, J. D. & DE VRIES, H. E. 2016. Acid Sphingomyelinase-Derived Ceramide Regulates ICAM-1 Function during T Cell Transmigration across Brain Endothelial Cells. *Journal of Immunology,* 196**,** 72-79.
36. POSTOW, M. A., CALLAHAN, M. K., BARKER, C. A., YAMADA, Y., YUAN, J., KITANO, S., MU, Z., RASALAN, T., ADAMOW, M., RITTER, E., SEDRAK, C., JUNGBLUTH, A. A., CHUA, R., YANG, A. S., ROMAN, R. A., ROSNER, S., BENSON, B., ALLISON, J. P., LESOKHIN, A. M., GNJATIC, S. & WOLCHOK, J. D. 2012. Immunologic correlates of the abscopal effect in a patient with melanoma. *N Engl J Med,* 366**,** 925-31.
37. PRITZL, C. J., SEO, Y. J., XIA, C., VIJAYAN, M., STOKES, Z. D. & HAHM, B. 2015. A ceramide analogue stimulates dendritic cells to promote T cell responses upon virus infections. *J Immunol,* 194**,** 4339-49.
38. SADDOUGHI, S. A., SONG, P. & OGRETMEN, B. 2008. Roles of bioactive sphingolipids in cancer biology and therapeutics. *Subcell Biochem,* 49**,** 413-40.
39. SHAO, C., FOLKARD, M., MICHAEL, B. D. & PRISE, K. M. 2004. Targeted cytoplasmic irradiation induces bystander responses. *Proc Natl Acad Sci U S A,* 101**,** 13495-500.
40. SMITH, E. L. & SCHUCHMAN, E. H. 2008. Acid sphingomyelinase overexpression enhances the antineoplastic effects of irradiation in vitro and in vivo. *Mol Ther,* 16**,** 1565-71.
41. STOFFEL, B., BAUER, P., NIX, M., DERES, K. & STOFFEL, W. 1998. Ceramide-independent CD28 and TCR signaling but reduced IL-2 secretion in T cells of acid sphingomyelinase-deficient mice. *Eur J Immunol,* 28**,** 874-80.
42. TAGUCHI, Y., KONDO, T., WATANABE, M., MIYAJI, M., UMEHARA, H., KOZUTSUMI, Y. & OKAZAKI, T. 2004. Interleukin-2-induced survival of natural killer (NK) cells involving phosphatidylinositol-3 kinase-dependent reduction of ceramide through acid sphingomyelinase, sphingomyelin synthase, and glucosylceramide synthase. *Blood,* 104**,** 3285-93.
43. TONINI, T., ROSSI, F. & CLAUDIO, P. P. 2003. Molecular basis of angiogenesis and cancer. *Oncogene,* 22**,** 6549-56.
44. VAN DER SCHANS, G. P. 1978. Gamma-ray induced double-strand breaks in DNA resulting from randomly-inflicted single-strand breaks: temporal local denaturation, a new radiation phenomenon? *Int J Radiat Biol Relat Stud Phys Chem Med,* 33**,** 105-20.
45. VAUPEL, P., KALLINOWSKI, F. & OKUNIEFF, P. 1989. Blood flow, oxygen and nutrient supply, and metabolic microenvironment of human tumors: a review. *Cancer Res,* 49**,** 6449-65.
46. VIGNALI, D. A. A., COLLISON, L. W. & WORKMAN, C. J. 2008. How regulatory T cells work. *Nature Reviews Immunology,* 8**,** 523-532.
47. ZHOU, Y., SALKER, M. S., WALKER, B., MUNZER, P., BORST, O., GAWAZ, M., GULBINS, E., SINGH, Y. & LANG, F. 2016. Acid Sphingomyelinase (ASM) is a Negative Regulator of Regulatory T Cell (Treg) Development. *Cell Physiol Biochem,* 39**,** 985-95.

9. Appendix

9.1 List of tables

9.2 List of figures

9.3 Abbreviations

ATP	adenosine triphosphate
Asm	acid sphingomyelinase
$Asm^{-/-}$	Asm deficient
APCs	antigen-presenting cells
CD	cluster of differentiation
CRT	calreticulin
CTLs	cytotoxic T-cells
DD	death domain
DNA	deoxyribonucleic acid
DSBs	double-strand breaks
DAMPs	damage-associated molecular patterns
DCs	dendritic cells
EMT	epithelial-mesenchymal transition
FADD	Fas associated with a death domain
HMGB1	high-mobility group box-1
ICAM-1	intercellular adhesion molecule 1
ICD	immunogenic cell death
LCB	long chain base
MDSCs	myeloid-derived suppressor cells
MHC1	major histocompatibility complex -1
MHC	major histocompatibility complex
NK	natural killers
NOS	nitric oxide synthase
ROS	reactive oxygen species
RNS	reactive nitrogen species
SPK	sphingosine kinase
SMase	sphingomyelinase
SMS	sphingomyelin synthase
S1P	sphingosine-1-phosphate
SSBs	single-strand breaks
SD	standard deviation
tAsm	transgenic Asm type
TIM	tumor inflammatory microenvironment
TME	tumor microenvironment

TAAs	tumor-associated antigens
TAM	tumor associated macrophages
Tregs	regulatory T-cells
Rt	room temperature
wt	wild type

Acknowledgments

I would like to express my sincere gratitude to my supervisors, Prof. Dr. Erich Gulbins and Dr. med Alexander Carpinteiro for their invaluable advice, continuous support, and patience during my MD study. Their immense knowledge and plentiful experience have encouraged me in all the time of my academic research and daily life. I would also like to thank Dr.rer.nat Stephanie Kadow for her technical support on my study. I would like to thank all the members in the Molecular Biology Institute. It is their kind help and support that have made my study and life in this lab a wonderful time. Finally, I would like to express my gratitude to my family. Without their tremendous understanding and encouragement in the past few years, it would be impossible for me to complete my study.

Curriculum Vitae

Der Lebenslauf ist in der Online-Version aus Gründen des Datenschutzes nicht enthalten.